

Pyridine-derived VEGFR-2 inhibitors: Rational design, synthesis, anticancer evaluations, in silico ADMET profile, and molecular docking

Nashwa M. Saleh¹ | Adel A.-H. Abdel-Rahman²  | Asmaa M. Omar² |
Mohamed M. Khalifa³  | Khaled El-Adl^{3,4} 

¹Department of Chemistry, Faculty of Science, Al-Azhar University (Girls Branch), Cairo, Egypt

²Department of Chemistry, Faculty of Science, Menoufia University, Shebin El-Koam, Egypt

³Department of Pharmaceutical Medicinal Chemistry and Drug Design, Faculty of Pharmacy (Boys), Al-Azhar University, Cairo, Egypt

⁴Department of Pharmaceutical Chemistry, Faculty of Pharmacy, Heliopolis University for Sustainable Development, Cairo, Egypt

Correspondence

Khaled El-Adl, Department of Pharmaceutical Medicinal Chemistry and Drug Design, Faculty of Pharmacy (Boys), Al-Azhar University, Nasr City 11884, Cairo, Egypt.
Email: eladlkhaled74@yahoo.com, eladlkhaled74@azhar.edu.eg, and khaled.eladl@hu.edu.eg

Nashwa M. Saleh, Department of Chemistry, Faculty of Science, Al-Azhar University (Girls Branch), Youssef Abbas Str., 6th District, Nassr City, PO Box 11754, Cairo 11765, Egypt.

Email: drnashwamostafa@azhar.edu.eg and drnashwa78@yahoo.com

Abstract

Novel pyridine-derived compounds (**5–19**) were designed and synthesized, and their anticancer activities were evaluated against HepG2 and MCF-7 cells, targeting the VEGFR-2 enzyme. Compounds **10**, **9**, **8**, and **15** were found to be the most potent derivatives against the two cancer cell lines, HepG2 and MCF-7, respectively, with IC_{50} = 4.25 and 6.08 μ M, 4.68 and 11.06 μ M, 4.34 and 10.29 μ M, and 6.37 and 12.83 μ M. Compound **10** displayed higher activity against HepG2 cells than sorafenib (IC_{50} = 9.18 and 5.47 μ M, respectively) and doxorubicin (IC_{50} = 7.94 and 8.07 μ M, respectively). It also showed higher activity than doxorubicin against MCF-7 cells, but lower activity than sorafenib. Compounds **9**, **8**, and **15** displayed higher activities than sorafenib and doxorubicin against HepG2 cells but exhibited lower activities against MCF-7 cells. Compound **10** potently inhibited VEGFR-2 at an IC_{50} value of 0.12 μ M, which is nearly equipotent to sorafenib (IC_{50} = 0.10 μ M). Compounds **8** and **9** exhibited very good activity with the same IC_{50} value of 0.13 μ M. The six most potent derivatives, **6**, **9**, **8**, **10**, **15**, and **18**, were tested for their cytotoxicity against normal Vero cells. Compounds **6**, **8**, **9**, **10**, **15**, and **18** are, respectively, 1.13, 3.74, 4.18, 3.64, 2.81, and 2.00 times more toxic to HepG2 and 2.06, 1.58, 1.76, 2.54, 1.40, and 2.69 times more toxic to MCF-7 breast cancer cells than in normal Vero cells.

KEYWORDS

2-cyanoacetohydrazone, anticancer agents, molecular docking, pyridines, VEGFR-2 inhibitors

1 | INTRODUCTION

Targeted cancer remedies have been developed in an attempt to avoid the side effects of standard chemotherapy. Inhibitors of signal transduction, angiogenesis inhibitors, apoptosis inducers, hormone therapies, modulators of gene expression, immunotherapies, and toxin delivery molecules are various targeted therapies that have been approved for

use in cancer treatment (<https://www.cancer.gov/about-cancer/treatment/types/targeted-therapies/targeted-therapies-fact-sheet>; <http://emedicine.medscape.com/article/1372666-overview>). Protein tyrosine kinases inhibitors (PTKIs) are among the first discovered and approved targeted drug therapies. Under both normal and pathological cell conditions, protein tyrosine kinases (PTKs) are well-established key players in controlling most cellular processes, including metabolism,

progression of the cell cycle, transcription, cytoskeletal rearrangement, cell movement, differentiation, and apoptosis.^[1-3] There are over 518 identified human protein kinases up-to-date encoded within the human genome, thus representing approximately 1.7% of all the human genes.^[1,3] Among these kinases is the vascular endothelial growth factor receptor-2 (VEGFR-2), which is well recognized to be associated with the progression and development of many types of cancers and angiogenesis. VEGF-2 is a key growth factor in tumor angiogenesis. A conformational change in VEGFR-2 was induced through the binding of VEGF to VEGFR-2, followed by receptor dimerization and phosphorylation of tyrosine residues. VEGFR-2 transmits its angiogenic signal via cell surface receptors located on the host vascular endothelial cells, which have intracellular TK activity. VEGF signaling through VEGFR-2 has been shown to play a key role in tumor angiogenesis regulation.^[4,5] Expression of VEGF is enhanced in several types of human tumors, and its expression levels are associated with poor prognosis and clinical stage in solid tumors patients.^[5-8] Therefore, VEGF/VEGFR-2 signaling is an attractive therapeutic target in cancer treatment. Consequently, the biological rationale and the effectiveness of small-molecule VEGFR-2 inhibitors in interfering with tumor-induced signals have been well established.^[9-12] On the basis of the different reported VEGFR-2 crystal structures, VEGFR-2 inhibitors can be classified into three main types: Type I inhibitors are able to block the active “DFG-in” conformation of the receptor by occupying the adenosine triphosphate (ATP)-binding region forming a hydrogen bond with the hinge region amino acid Cys919. Type II inhibitors occupy the ATP-binding site and extend over the gate area into the adjacent allosteric hydrophobic back pocket of the inactive “DFG-out” conformation. Type III inhibitors accommodate the allosteric hydrophobic back pocket of VEGFR-2 in the inactive “DFG-out” conformation, blocking the receptor through hydrophobic interactions.^[13]

Study of SAR and common pharmacophoric features shared by, for example, sorafenib (I) and lenvatinib (II),^[14] and various VEGFR-2 inhibitors revealed that most VEGFR-2 inhibitors shared four main pharmacophoric features^[15,16] (Figure 1), which are (1) a hinge region binding moiety “head,” which is a heterocycle that occupies the adenine region in the ATP-binding pocket with H-bond donor and/or

acceptor capabilities to interact with Cys919 (colored red), (2) a “linker,” which is a segment of three to four chemical bonds that extends over the gatekeeper residue (colored green), (3) a hydrogen-bonding moiety that is required to achieve hydrogen bond interaction with the Asp1046 in the conserved DFG motif and Glu885 of the α C helix (colored purple), and (4) a “tail” segment typically consisting of a hydrophobic moiety that occupies the allosteric hydrophobic back pocket created by the DFG-out flip (colored blue).^[16,17]

As shown in Figure 2, the pyridine skeleton had been widely used in VEGFR inhibitors. Small-molecule ATP-competitive inhibitors of VEGFR-2 (Type I inhibitors) based on a pyridine nucleus have demonstrated high activity as antitumor agents like apatinib (III), motesanib (IV), and sorafenib (I), as displayed in Figure 2.^[17-21] In 2020, AbdelHaleem et al.^[22] designed a series of new pyridine scaffolds that were biologically evaluated for their inhibitory activity against VEGFR-2. The most potent compound (V) (Figure 2) displayed very good anticancer activities against two prostate cancer cell lines, namely PC3 and DU145, and two breast cancer cell lines, namely MCF-7 and MDA-MB435, with IC₅₀ values of 55, 8.5, 0.5, and 96 nM, respectively. It also inhibited VEGFR-2 at an IC₅₀ value of 0.19 nM.^[22] Moreover, the bioisostere pyrimidine derivative compound (VI) (Figure 2) displayed very good anticancer activities and potently inhibited VEGFR-2 at an IC₅₀ value of 1.97 μ M.^[23]

The emergence of tumor resistance to the effect of currently clinically used small-molecule tyrosine kinases inhibitors (TKIs) opens the door for the exploration of new chemotypes. The chemical entities bearing a 3-cyano-4-aryl-pyridin-2-one moiety or its 2-amino bioisostere have received considerable attention owing to their ability to elicit cytotoxic antiproliferative activities employing various mechanisms of actions specially kinase inhibition mechanism.^[22,24-26]

In view of the above-mentioned findings and based on our continuous efforts to develop new anticancer agents,^[27-29] especially VEGFR-2 inhibitors,^[30-39] it is deemed of interest to initiate a research work directed at the design and synthesis of a new series of potential pyridine-derived cytotoxic compounds. The design of these

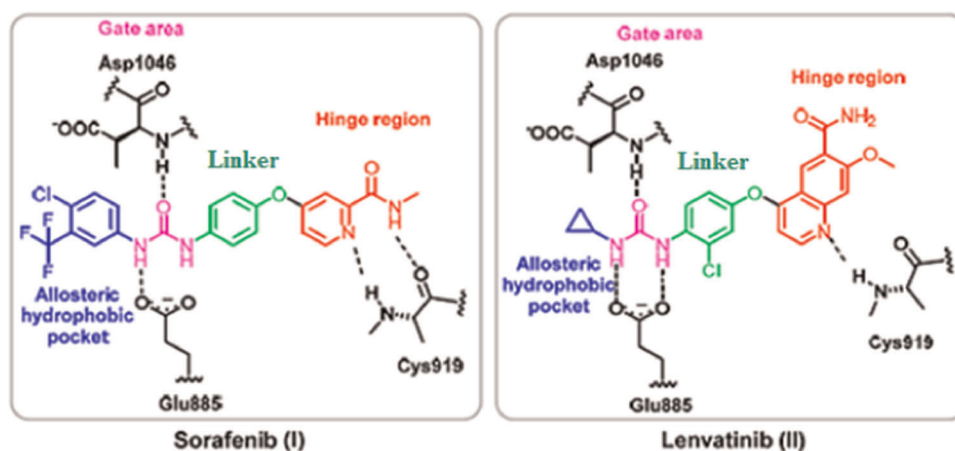


FIGURE 1 Representation of type II vascular endothelial growth factor receptor-2 (VEGFR-2) inhibitors in the VEGFR-2 active site

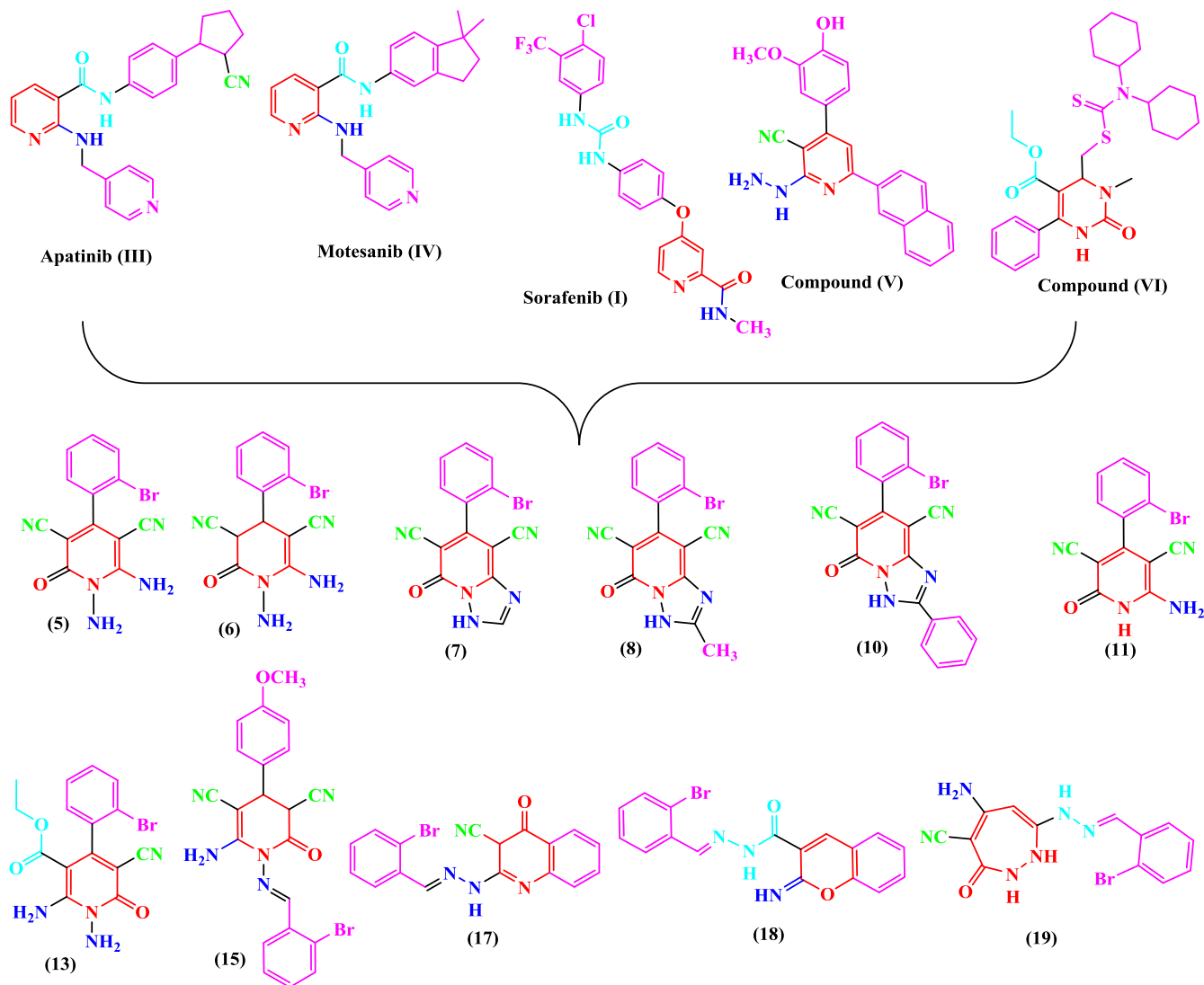


FIGURE 2 Reported pyridine-derived vascular endothelial growth factor receptor-2 inhibitors and our derivatives

derivatives was directed by the idea of cross-hybridization with the pharmacophoric elements of the cytotoxic agents: sorafenib, lenvatinib, apatinib, motesanib, compound (V), and compound (VI) (Figure 2). The pyridine bioisosteres, pyran and 1,2-diazepine scaffolds, were introduced to yield derivatives of general structures 22 and 23 (Figure 2). These derivatives are designed as antiproliferative agents with potential ATP-competitive kinase inhibition (Type I inhibitors) where the pyridine ring will occupy the ATP-binding region forming a hydrogen bond with the hinge region amino acid Cys919. The designed hydrophobic moieties extend to occupy different hydrophobic pockets to increase binding affinities toward the VEGFR-2 receptor.

Multiple structural manipulations were performed to study SAR implications of these transformations on the studied pharmacological activities of these derivatives. The adopted molecular manipulations and design strategy involved varying substituents with different hydrophobic and electronic nature. In general, the designed compounds were synthesized and evaluated

for their *in vitro* antiproliferative activities against two human tumor cell lines, namely hepatocellular carcinoma (HCC) type (HepG2) and breast cancer (Michigan Cancer Foundation-7 [MCF-7]).

VEGFR-2 was reported to be substantially upregulated in HepG2 cells in a dose-dependent manner with the stimulation of the hepatocyte growth factor (HGF), which is involved in cell proliferation, invasion, and angiogenesis of hepatocellular carcinoma (HCH).^[40–42] Blockade of VEGFR-2 signaling revealed a marked inhibition on both the growth and metastasis of HCC. Also, VEGFR-2 was found to be crucial to cell survival and regulates endothelial differentiation in the breast cancer cells (MCF-7).^[42,43] Overexpression of VEGFR-2 receptors in breast cancer cells has been documented to be a contributor in resistance of such cancer type to the chemotherapeutic effect of tamoxifen.^[44]

Moreover, the most potent compounds were tested for their *in vitro* cytotoxicity against the normal Vero cells. The obtained results prompted us to make further examinations to achieve deep insight into the mechanism of action of the synthesized compounds.

Molecular docking studies were carried out to assess the binding interactions of the target compounds with VEGFR-2 active sites. Moreover, the most active cytotoxic compounds that showed promising IC_{50} values against the two cancer cell lines were subjected to further investigation for their tyrosine kinase inhibitory activities against VEGFR-2.

2 | RESULTS AND DISCUSSION

2.1 | Rationale and structure-based design

Our pyridine derivatives have the essential pharmacophoric features of a VEGFR-2 inhibitor. The presence of pyridine hetero ring alone as in compound 15 and/or the pyridine ring fused to triazole moiety as in compound 10 were designed to replace the pyridine ring of the reference ligand sorafenib. These moieties were designed to occupy the ATP-binding pocket of the VEGFR-2 receptors. The pyridine moiety in compound 15 occupied the hydrophobic ATP-binding pocket formed by Leu1035, Cys919, Phe918, Glu917, Val848, Leu840, and Arg833 (Figure 3). The triazolo[1,5-*a*]pyridine moiety in compound 10 occupied the hydrophobic ATP-binding pocket also (Figure 4).

2.2 | Chemistry

The synthetic strategies followed to achieve the target compounds are seen in Schemes 1–4. Synthesis of Schiff's base 4 as a key intermediate^[45–47] in excellent yield was carried out by condensation of equimolar amounts of *O*-bromobenzaldehyde 1 with 2-cyanoacetohydrazide 3^[45–47] in absolute ethanol with few drops of glacial acetic acid as a catalyst (Scheme 1). The infrared (IR) spectrum of compound 4 revealed a characteristic absorption band at 3190 cm^{-1} (NH), 2264 cm^{-1} ($C\equiv N$), and 1675 cm^{-1} ($C=O$). Also, the ^1H NMR (nuclear magnetic resonance) spectrum of compound 4 showed the presence of two singlet signals at 4.22

and 11.95 ppm attributed to the CH_2 and NH, respectively, and singlet signal at 8.33 ppm corresponding to ($\text{CH}=\text{N}$) group. In addition, the ^{13}C NMR spectrum showed characteristic signals at δ 24.85 for (CH_2), 116.45 for ($\text{C}\equiv\text{N}$), and 159.53 and 192.18 ppm assigned to ($\text{CH}=\text{N}$) and ($\text{C}=\text{O}$), respectively. The targeted compound 1,6-diamino-4-(2-bromophenyl)-2-oxo-1,2-dihydropyridine-3,5-dicarbonitrile 5 was synthesized by two pathways (Scheme 1). The first pathway was through the formation of the key intermediate *N'*-(2-bromobenzylidene)-2-cyanoacetohydrazide 4 with malononitrile in the presence of piperidine as a catalyst. The second pathway consists of a condensation of *O*-bromobenzaldehyde with the active methylene of malononitrile to afford 2-(2-bromobenzylidene)malononitrile 2. An alcoholic solution of 2 and 3 was heated under reflux to obtain the targeted compound 5 (Scheme 1). The proposed mechanism of formation of 1,6-diamino-pyridine-3,5-dicarbonitrile derivative (5) is illustrated in Figure 5.^[48,49]

The structure of compound 5 was proved on the basis of analytical and spectral data. Thus, the IR spectrum of compound 5 showed characteristic absorption bands at 3407 , 3313 , and 3210 cm^{-1} due to two amino groups (2 NH_2), 2207 and 1676 cm^{-1} for two cyano groups ($2\text{ C}\equiv\text{N}$) and carbonyl group ($\text{C}=\text{O}$), respectively. Also, the ^1H NMR spectrum of compound 5 revealed the presence of two singlet signals that were exchangeable with D_2O at δ 5.70 and 8.60 ppm due to the *N*- NH_2 and *C*- NH_2 protons, respectively. As a result of the difference in nucleophilicity, hydrazide β -nitrogen (*N*- NH_2) reacts faster with the electron-deficient carbon than the second amino group (*C*- NH_2). In addition, the ^{13}C NMR spectrum showed characteristic signals at 75.40 and 114.59 ppm for C^3 and C^5 of pyridine, 116.01 and 116.41 ppm for two cyano groups, 159.48 and 166.93 ppm assigned to ($\text{C}-\text{NH}_2$) and ($\text{C}=\text{O}$), respectively. Compound 5 was further indicated from its mass spectrum that showed the molecular ion peak at m/z 330, which agreed with the molecular formula $\text{C}_{13}\text{H}_8\text{BrN}_5\text{O}$ and supported the identity of the new compound 4-(2-bromophenyl)-2-oxo-1,2,3,4-tetrahydropyridine-3,5-dicarbonitrile (5). Conformation of the structure of 6 is carried out by careful data of its spectral analysis. Its ^1H NMR spectrum showed characteristic signals at δ 3.03 and 3.06 ppm for $\text{C}_4\text{-H}$ and $\text{C}_3\text{-H}$ of the

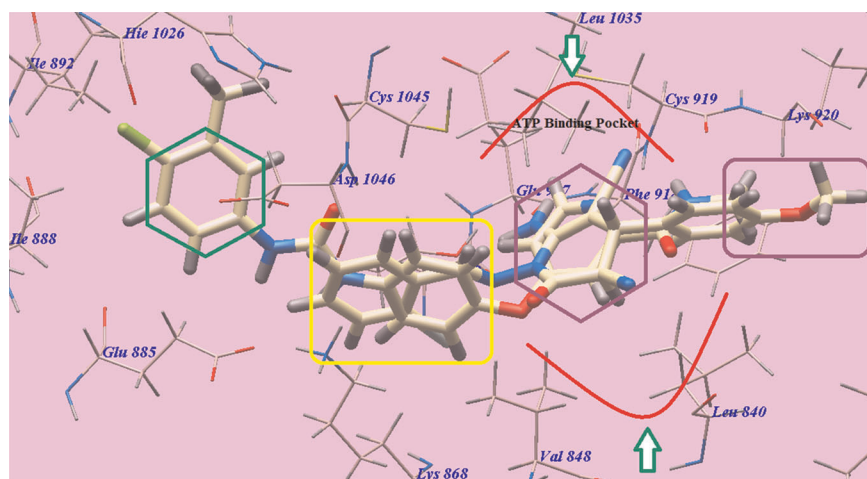
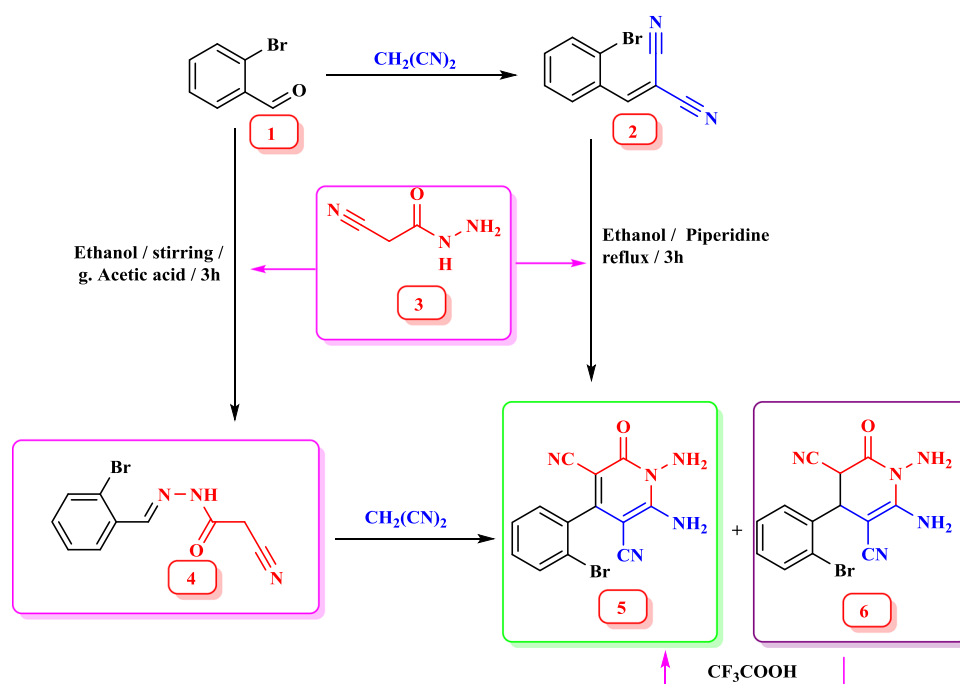
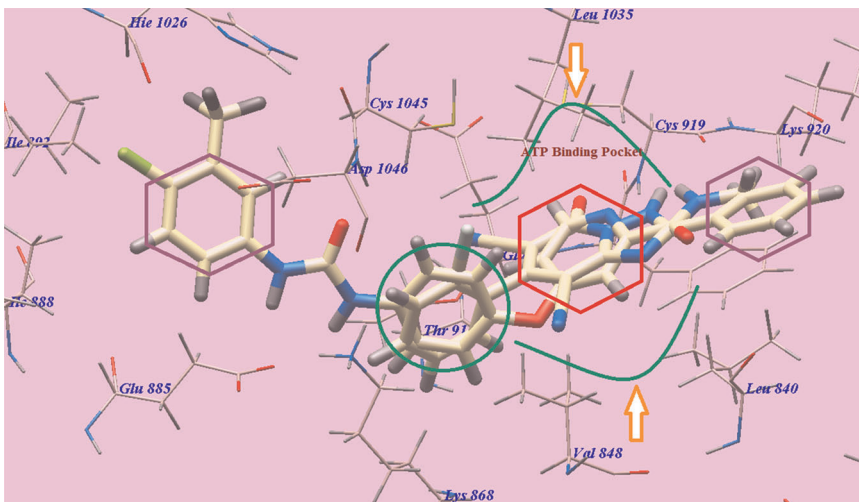


FIGURE 3 Superimposition of compound 15 and sorafenib inside the binding pocket of vascular endothelial growth factor receptor-2

FIGURE 4 Superimposition of compound **10** and sorafenib inside the binding pocket of vascular endothelial growth factor receptor-2



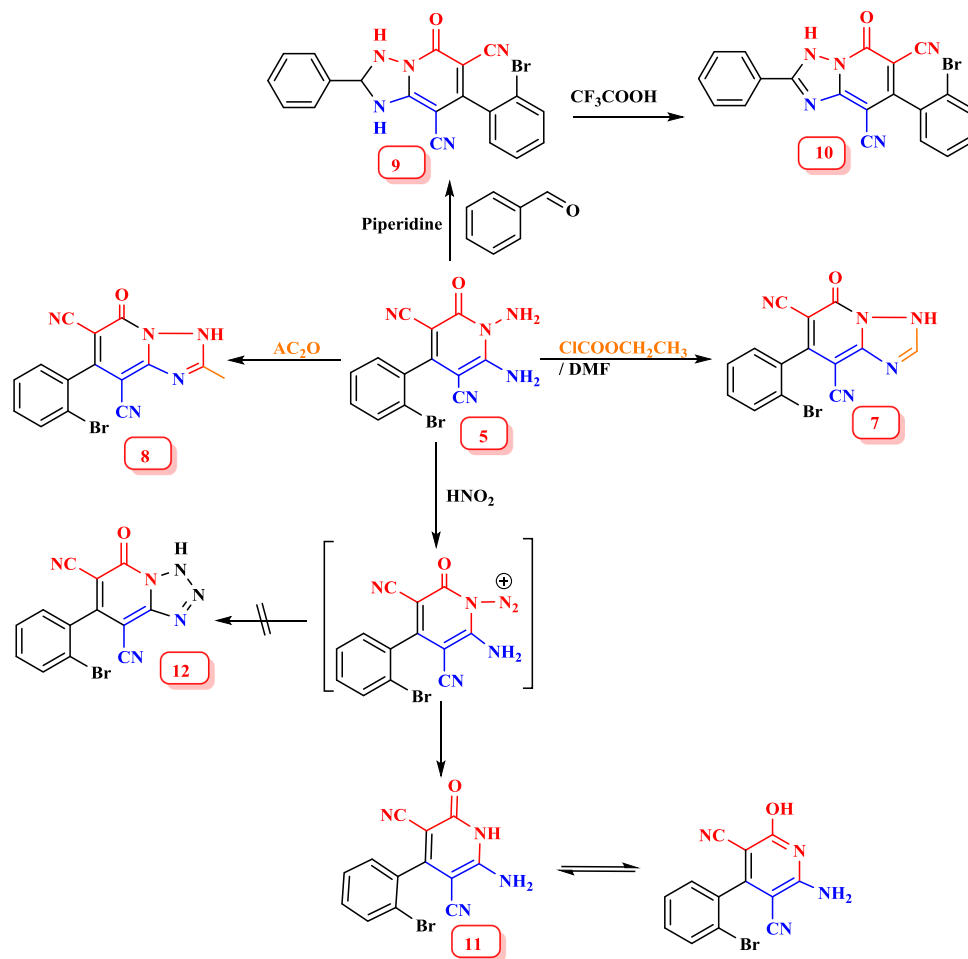
SCHEME 1 Synthetic route for the formation of 1,6-diaminopyridones **5** and **6**

pyridine ring. O-Amino heterocyclic carboxamides are a good nucleophilic center to produce fused nitrogen heterocyclic rings.^[50,51]

Cyclization of **5** with ethyl chloroformate was carried out to yield 7-(2-bromophenyl)-5-oxo-3,5-dihydro-[1,2,4]triazolo[1,5-*a*]pyridine-6,8-dicarbonitrile **7**. New triazolopyridone is formed by the reaction of the starting compound **5** with some mono-electrophilic reagents such as acetic anhydride. Heterocyclization of compound **5** with acetic anhydride under reflux yielded 7-(2-bromophenyl)-2-methyl-5-oxo-3,5-dihydro-[1,2,4]triazolo[1,5-*a*]pyridine-6,8-dicarbonitrile **8** (Scheme 2). Formation of compound **8** occurs via a nucleophilic attack of the exocyclic amino group of **5** on the keto group of 1,3-dicarbonyls, followed by triazole ring closure through intramolecular cyclization by the loss of one molecule of

acetic acid and one molecule of water (Scheme 2). The IR and ¹H NMR spectra of compound **8** confirmed the absence of the two NH₂ groups. The IR spectrum showed characteristic absorption bands at 1690 cm⁻¹ for (C=O pyridone) and 2126 cm⁻¹ for (2 C≡N). The ¹H NMR spectrum revealed the presence of methyl group at δ 1.29 (CH₃ triazole) and at 23.05 ppm in ¹³C NMR spectra.

Reaction of product **5** with benzaldehyde afforded 7-(2-bromophenyl)-5-oxo-2-phenyl-1,2,3,5-tetrahydro-[1,2,4]triazolo[1,5-*a*]pyridine-6,8-dicarbonitrile (**9**) (Scheme 2). ¹H NMR spectral data for compound **9** showed singlet signal at δ 4.21 ppm, assigned to CH-triazole, in addition to two singlet signals at δ 9.26 and 10.71 ppm, indicating the presence of two NH groups. The [1,2,4]triazolo[1,5-*a*]pyridine derivative **10** was obtained by stirring of **9**



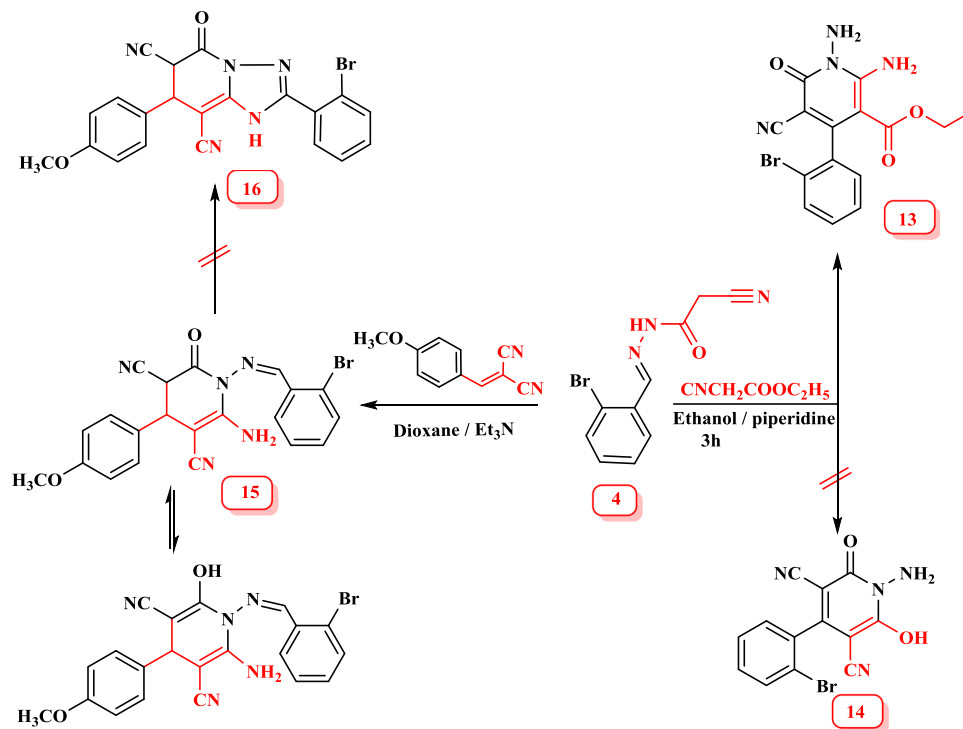
SCHEME 2 Synthetic route for the formation of compounds 5–11

with trifluoroacetic acid, as shown in (Scheme 2). *N*-Deamination of the diaminopyridinone derivative **5** was carried out under mild conditions. ^1H NMR spectra of **10** revealed the absence of the methylene proton signals and presence of one deuterium oxide exchangeable signal at δ 8.46 ppm for NH. ^{13}C NMR spectrum of these compounds exhibited two signals for cyano group at 116.26 and 116.64 ppm, as well as Ar-C at a range of 128.78–148.52 ppm; finally, C=O appeared at 166.36 ppm.

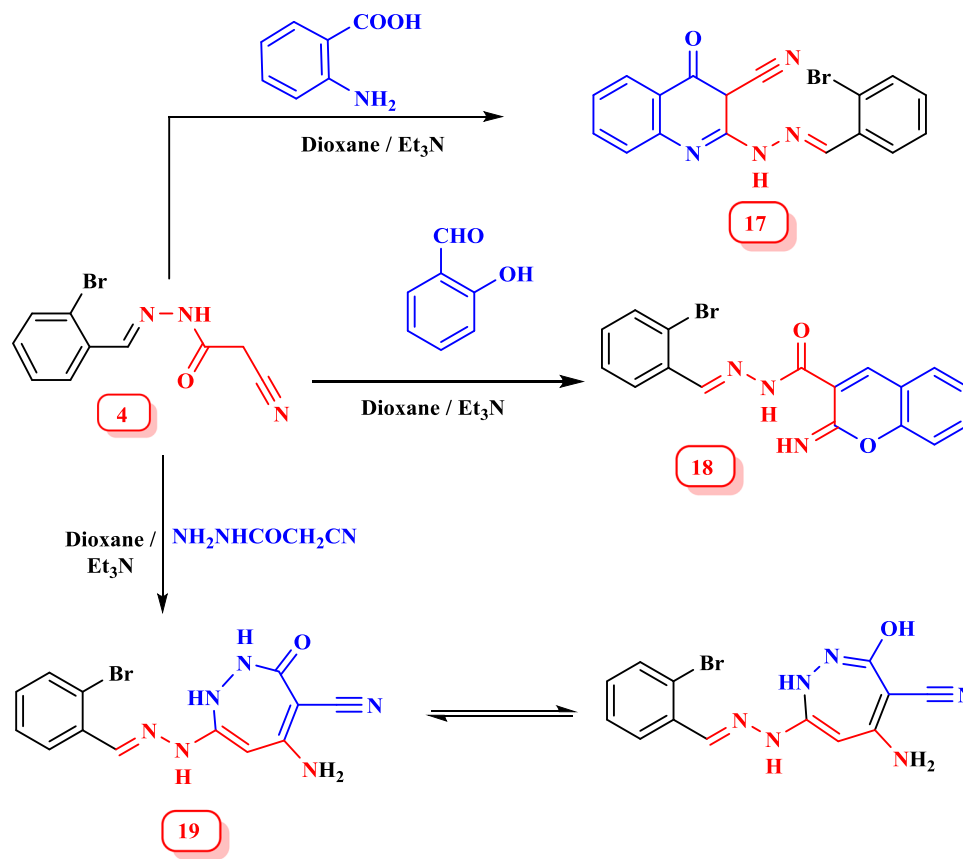
Thus, upon treating **5** with sodium nitrile in aqueous acetic acid, the expected product **11** was obtained, rather than the unexpected tetrazolopyridine derivatives **12** (Scheme 2). Elemental analysis and spectral data confirmed the proposed structure of **11**. Its IR spectrum showed stretching vibration bands for NH/NH₂ around 3300 and 3406 cm^{-1} , cyano group at 2210 cm^{-1} , and C=O at 1691 cm^{-1} , respectively.

However, reaction of **4** with ethyl cyanoacetate in the presence of triethylamine afforded ethyl-1,2-diamino-4-(2-bromophenyl)-5-cyano-6-oxo-1,6-dihydropyridine-3-carboxylate **13** rather than 1-amino-4-argio-6-hydroxy-2-oxo-1,2-dihydropyridine-3,5-dicarbonitrile **14** (Scheme 3). The structure of compound **13** was proved on the basis of analytical and spectral data. The IR spectrum of **13** revealed a characteristic absorption band at 3399 cm^{-1} and 3290 cm^{-1} due to bands of amino groups (2 NH₂),

2216 cm^{-1} for cyano groups (C≡N), and presence of new absorption bands at 1651 cm^{-1} due to a carbonyl group (C=O). Also, the ^1H NMR spectrum of compound **13** revealed triplet and quarter signals at 1.19 and 4.30 ppm attributed to the ester proton and the presence of two singlet signals that were exchangeable with D₂O at 5.70 and 9.05 ppm due to the *N*-NH₂ and *C*-NH₂ protons, respectively. ^{13}C NMR spectrum was characterized by signals at 159.20 and 165.82 ppm corresponding to two carbonyl carbon atoms, signals at 116.39 ppm assigned to (C-CN), and 120.75 ppm assigned to the cyano group. Treating **4** with *p*-methoxybenzylidene malononitrile in the presence of triethylamine gave 6-amino-1-[(2-bromobenzylidene)amino]-4-(4-methoxyphenyl)-2-oxo-1,2,3,4-tetrahydropyridine-3,5-dicarbonitrile (**15**) (Scheme 3). The reaction may proceed as nucleophilic addition to the active double bond, followed by cycloaddition of the amino group of (NH-NH₂) with concomitant dehydration to produce the target compound **15**, which appears more likely than compound **16** on the basis of elemental analysis and spectral data. IR spectrum of **15** revealed characteristic absorption bands at 3347 and 3202 cm^{-1} due to bands of amino groups (NH₂), 2215 cm^{-1} for cyano groups (C≡N), and presence of new absorption bands at 1699 cm^{-1} assignable to a carbonyl group (C=O). The ^1H NMR spectrum of compound **15** showed singlet signals at



SCHEME 3 Synthetic route for the formation of the expected products 13 and 15



SCHEME 4 Cyclization of 4 with different nucleophilic reagents to obtain compounds 17–19

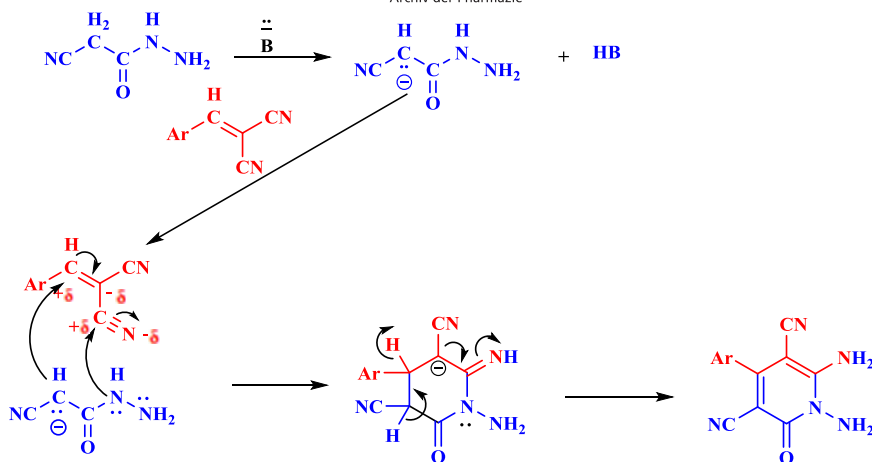


FIGURE 5 The proposed mechanism of formation of 1,6-diamino-pyridine-3,5-dicarbonitrile derivative 5

3.22 ppm attributed to methoxy protons and the presence of singlet signal that was exchangeable with D_2O at δ 5.62 ppm due to the presence of amino group, providing good evidence for the suggested open chain structure **15** instead of the cyclic [1,2,4] triazolo structure **16**. Furthermore, its ^{13}C NMR spectrum exhibited three signals at 116.16, 117.04, and 157.09 ppm due to cyano and carbonyl groups, respectively, in addition to signals between 114.17 and 133.87 ppm corresponding to aromatic carbons.

In turn, quinoline derivative **17** was obtained upon treating **4** with anthranilic acid in refluxing dioxane and triethylamine (Scheme 4). The chemical structure of **17** was established from its spectral data that showed bands characteristic for $C=N$, NH , and $C=O$ groups (Scheme 4). Cyclocondensation of acetohydrazone (**4**) with salicylaldehyde in dioxane and triethylamine as a base achieved the chromene derivative **18** (Scheme 4). The IR spectra provided the presence of sharp stretching absorption bands characteristic for NH , CO , and $C=N$ group frequencies and the absence of $C\equiv N$ absorption and carbonyl band for δ -lactone, which confirm the imino coumarin structure. IR spectrum of compound **18** exhibited the characteristic absorption bands as follows: 3199 and 1614 cm^{-1} for NH , and $C=N$, respectively. The 1H NMR spectrum of compound **18** shed further light on the assigned structure as it displayed the characteristic signals for NH , $CH=N$, and aromatic protons. The 1H NMR spectrum provided two exchangeable signals due to NH protons. The higher δ values of $NHCO$ signal at 11.95 ppm and singlet signals for imino $=NH$ proton at 8.94 ppm were observed. The formation of chromenone derivative **18** was attributed to the initial Knoevenagel condensation of the active methylene of compound **4** with aldehydic carbonyl group of salicylaldehyde, followed by an intramolecular cyclization via nucleophilic addition of the phenolic OH group to the cyano function to furnish the target compound (Scheme 4). When **4** was allowed to react with 2-cyanoacetohydrazone, it gave 1,2-diazepine derivatives **19** (Scheme 4). The assignment of the structure of compound **19** was inferred from their spectroscopic data. Thus, the IR spectrum displayed the stretching absorption bands for the NH_2 group at

3192 and 3404 cm^{-1} and the $C\equiv N$ group at 2213 cm^{-1} . The 1H NMR spectrum of compound **19** showed the mixture of keto-enol tautomers.

2.3 | Docking studies

Molsoft software was used in all modeling experiments. Each experiment used VEGFR-2 downloaded from the Brookhaven Protein Data Bank (PDB ID 3B8Q).^[22]

The binding site of the VEGFR-2 receptor reveals a large space bounded by a membrane-binding domain, which serves as an entry channel for the substrate to the active site (Figure 6). All studied ligands have a similar position and orientation inside the recognized active site. Most of our derivatives had a good binding affinity toward the VEGFR-2 receptor, which is explained through the obtained results of free energy of binding (ΔG) (Table 1).

The proposed binding mode of sorafenib revealed an affinity value of -84.12 kcal/mol and four H-bonds. The *N*-methylpicolinamide moiety was stabilized by the formation of two H-bonds with the essential amino acid Cys919 where the pyridine N atom formed one H-bond with the NH of Cys919 (2.94 Å), whereas its NH group formed one H-bond with the carbonyl of Cys919 (2.07 Å). The urea linker formed one H-bond with the key amino acid Glu885 (2.40 Å) through its NH group and one H-bond with Asp1046 (2.08 Å) through its carbonyl group. The *N*-methylpicolinamide moiety occupied the hydrophobic ATP-binding pocket formed by Leu1035, Lys920, Cys919, Phe918, Glu917, Val848, and Leu840. Moreover, the central phenyl ring occupied the hydrophobic pocket formed by Cys1045, Leu1035, Thr916, Lys868, and Val848. Furthermore, the hydrophobic 3-trifluoromethyl-4-chlorophenyl moiety attached to the urea linker occupied the hydrophobic pocket formed by Asp1046, Cys1045, His1026, Ile892, Ile888, and Glu885 (Figure 7).

The proposed binding mode of compound **10** is virtually the same as that of sorafenib. It revealed an affinity value of -84.08 kcal/mol and three H-bonds. The triazolo[1,5-*a*]pyridine moiety was stabilized by the formation of two H-bonds with Cys919. The NH at

FIGURE 6 Superimposition of some docked compounds inside the binding pocket of vascular endothelial growth factor receptor-2

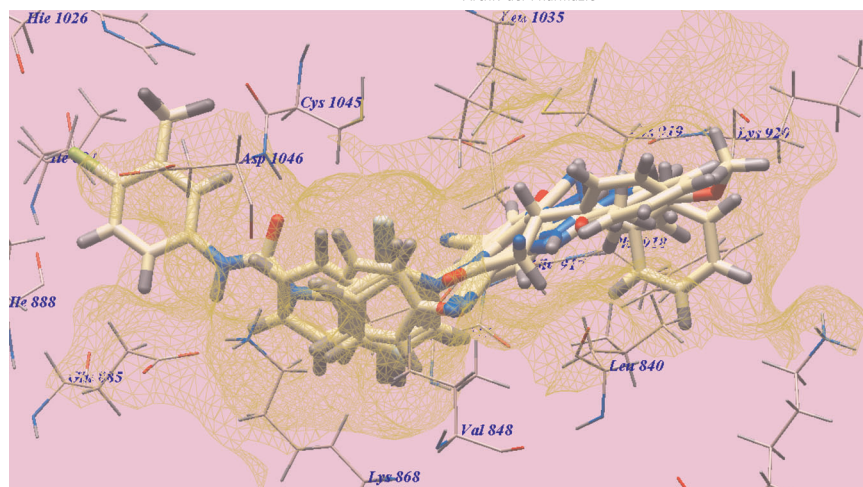


TABLE 1 The calculated free energy of binding (ΔG in kcal/mole) for the ligands

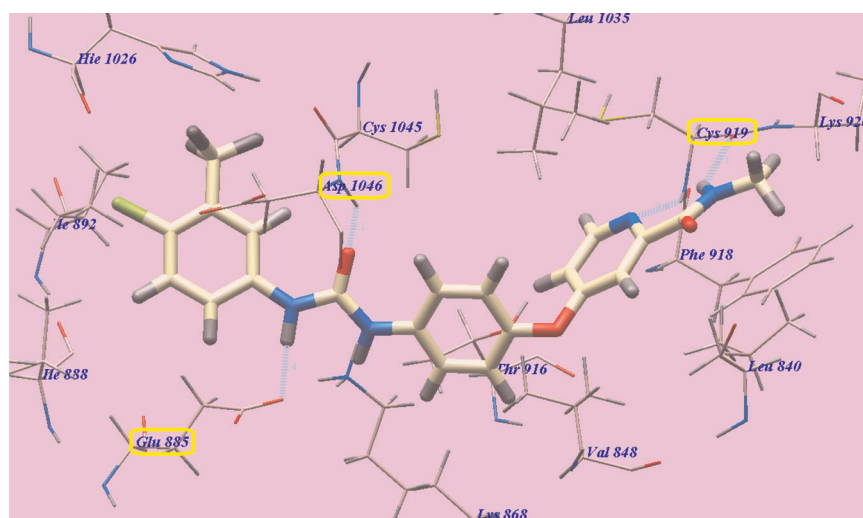
Compound	ΔG (kcal/mol)	Compound	ΔG (kcal/mol)
5	-78.95	13	-69.05
6	-77.31	15	-81.76
7	-69.56	17	-79.13
8	-83.72	18	-80.08
9	-81.89	19	-69.75
10	-84.08	Sorafenib	-86.12
11	-70.16		

position-3 formed one H-bond with the carbonyl of Cys919 with a distance of 2.37 Å, whereas the carbonyl group at position-5 formed another H-bond with the NH group of Cys919 (2.08 Å). Moreover, the CN group at position-6 formed the third H-bond with Thr916 (1.36 Å). The phenyl moiety at position-2 occupied the hydrophobic groove formed by Lys920, Phe918, and Leu840. The triazolo[1,5-*a*]

pyridine moiety occupied the hydrophobic ATP-binding pocket formed by Cys1045, Leu1035, Lys920, Cys919, Phe918, Glu917, Val848, and Leu840. Furthermore, the 2-bromophenyl ring attached at position-7 occupied the hydrophobic groove formed by Asp1046, Cys1045, His1026, Thr916, Lys868, and Val848 (Figure 8). These interactions of compound 10 may explain its high anticancer activity.

The proposed binding mode of compound 8 is virtually the same as that of 10. It revealed an affinity value of -83.72 kcal/mol and three H-bonds. The triazolo[1,5-*a*]pyridine moiety was stabilized by the formation of two H-bonds with Cys919. The NH at position-3 formed one H-bond with the carbonyl of Cys919 with a distance of 2.31 Å, whereas the carbonyl group at position-5 formed another H-bond with the NH group of Cys919 (1.94 Å). Moreover, the CN group at position-6 formed the third H-bond with Thr916 (1.40 Å). The methyl group at position-2 occupied the hydrophobic groove formed by Lys920, Phe918, and Leu840. The triazolo[1,5-*a*]pyridine moiety occupied the hydrophobic ATP-binding pocket formed by Cys1045, Leu1035, Lys920, Cys919, Phe918, Glu917, Val848, and Leu840. Furthermore, the 2-bromophenyl ring attached at position-7 occupied the the

FIGURE 7 Predicted binding mode for sorafenib with vascular endothelial growth factor receptor-2. H-bonded atoms are indicated by dotted lines



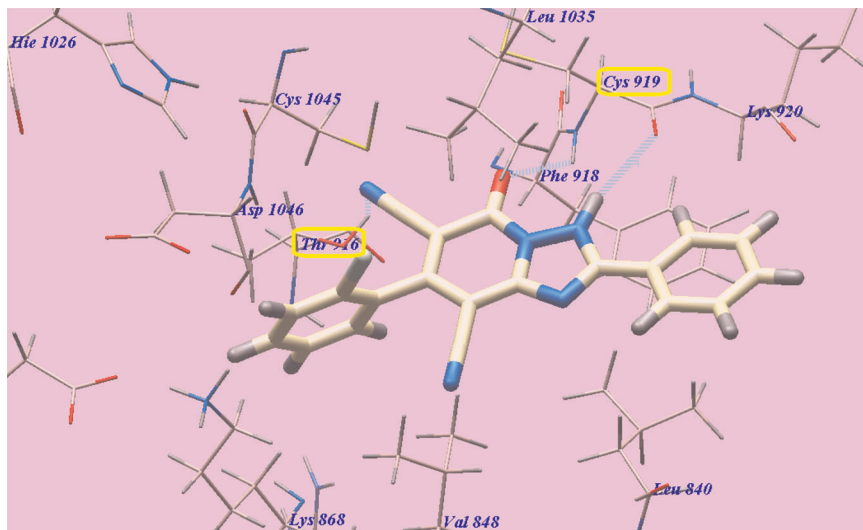


FIGURE 8 Predicted binding mode for **10** with vascular endothelial growth factor receptor-2

hydrophobic groove formed by Asp1046, Cys1045, His1026, Thr916, Lys868, and Val848 (Figure 9). These interactions of compound **8** may explain its high anticancer activity.

The proposed binding mode of compound **15** is virtually the same as that of **10**. It revealed an affinity value of -83.13 kcal/mol and three H-bonds. The pyridine ring was stabilized by the formation of three H-bonds. The NH_2 at position-6 formed two H-bonds with Thr916 (2.48 \AA) and Glu917 (2.31 \AA). Moreover, the CN group at position-5 formed the third H-bond with Cys919 (1.50 \AA). The 4-methoxyphenyl moiety at position-3 occupied the hydrophobic groove formed by Lys920, Cys919, Phe918, Leu840, and Lys838. The pyridine moiety occupied the hydrophobic ATP-binding pocket formed by Leu1035, Cys919, Phe918, Glu917, Val848, Leu840, and Arg833. Furthermore, the 2-bromophenyl ring attached at position-7 occupied the hydrophobic groove formed by Asp1046, Cys1045, His1026, Thre916, Glu885, Lys868, and Val848 (Figure 10). These interactions of compound **15** may explain its high anticancer activity.

2.4 | In vitro cytotoxic activity

Antiproliferative activity of the newly synthesized derivatives **5–19** was examined against two human tumor cell lines, namely, hepatocellular carcinoma (HepG2) and breast cancer (MCF-7), using 3-[4,5-dimethylthiazol-2-yl]-2,5-diphenyltetrazolium bromide colorimetric assay, as described by El-Helby et al.^[52] Sorafenib and doxorubicin were incorporated in the experiments as reference cytotoxic drugs. The results were expressed as growth inhibitory concentration (IC_{50}) values, and they are summarized in Table 2. From the obtained results, it was explicated that most of the prepared compounds displayed excellent-to-good growth inhibitory activity against the tested cancer cell lines. In particular, compounds **10**, **9**, **8**, and **15** were found to be the most potent derivatives over all the tested compounds against the two HepG2 and MCF-7 cancer cell lines with $\text{IC}_{50} = 4.25 \pm 0.03$, $6.08 \pm 0.06 \mu\text{M}$, 4.68 ± 0.06 , $11.06 \pm 0.09 \mu\text{M}$, 4.34 ± 0.04 ,

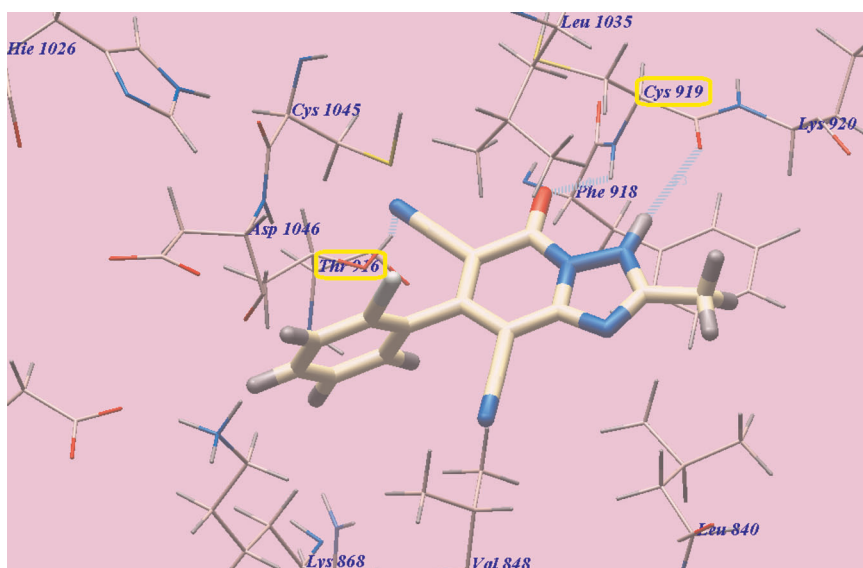
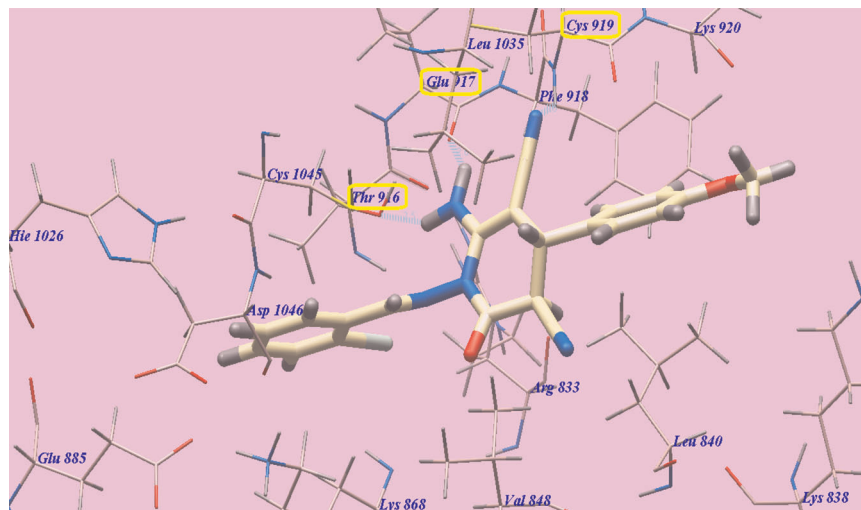


FIGURE 9 Predicted binding mode for **8** with vascular endothelial growth factor receptor-2

FIGURE 10 Predicted binding mode for **15** with vascular endothelial growth factor receptor-2



10.29 ± 0.09 μM, 6.37 ± 0.06, and 12.83 ± 0.13 μM, respectively. Compound **10** exhibited higher activity against HepG2 than sorafenib (IC₅₀ = 9.18 ± 0.6 and 5.47 ± 0.3 μM, respectively) and doxorubicin (IC₅₀ = 7.94 ± 0.6 and 8.07 ± 0.8 μM, respectively). It also exhibited higher activity than doxorubicin against MCF-7 cancer cell lines but lower than sorafenib. Compounds **9**, **8**, and **15** exhibited higher activities than sorafenib and doxorubicin against HepG2 but exhibited lower activities against MCF-7 cancer cell lines.

With respect to the HepG2 hepatocellular carcinoma cell line, compounds **18**, **17**, **5**, **6**, and **11** displayed very good anticancer activities with IC₅₀ = 11.79 ± 0.13, 12.90 ± 0.61, 14.29 ± 0.13, 16.57 ± 0.15, and 19.21 ± 0.16 μM, respectively, whereas compounds **19**, **7**, and **13**, with IC₅₀ = 23.55 ± 0.24, 28.20 ± 0.25, and 30.33 ± 0.29 μM, respectively, displayed good cytotoxicity.

Cytotoxicity evaluation against MCF-7 cell line revealed that compounds **18**, **6**, **5**, **17**, and **13** displayed very good anticancer activities with IC₅₀ = 8.77 ± 0.07, 8.85 ± 0.06, 11.37 ± 0.11,

TABLE 2 In vitro cytotoxic activities of the newly synthesized compounds against HepG2, MCF-7, and Vero cell lines, and VEGFR-2 kinase assay

Compound	IC ₅₀ (μM)			
	HepG2	MCF-7	Vero cells	VEGFR-2
5	14.29 ± 0.13	11.37 ± 0.11	NT	0.19 ± 0.02
6	16.57 ± 0.15	8.85 ± 0.06	18.22 ± 0.16	0.19 ± 0.02
7	28.20 ± 0.25	24.52 ± 0.24	NT	0.29 ± 0.02
8	4.68 ± 0.06	11.06 ± 0.09	17.50 ± 0.16	0.13 ± 0.02
9	4.34 ± 0.04	10.29 ± 0.09	18.14 ± 0.17	0.13 ± 0.02
10	4.25 ± 0.03	6.08 ± 0.06	15.45 ± 0.16	0.12 ± 0.01
11	19.21 ± 0.16	23.84 ± 0.22	NT	0.25 ± 0.03
13	30.33 ± 0.29	20.58 ± 0.21	NT	0.33 ± 0.01
15	6.37 ± 0.06	12.83 ± 0.13	17.93 ± 0.22	0.14 ± 0.05
17	12.90 ± 0.61	17.65 ± 0.16	NT	0.19 ± 0.02
18	11.79 ± 0.13	8.77 ± 0.07	23.59 ± 0.12	0.16 ± 0.02
19	23.55 ± 0.24	22.39 ± 0.21	NT	0.25 ± 0.02
Sorafenib	9.18 ± 0.6	5.47 ± 0.3	NT	0.10 ± 0.02
Doxorubicin	7.94 ± 0.6	8.07 ± 0.8	NT	NT

Note: IC₅₀ values are the mean ± SD of three separate experiments.

Abbreviations: HepG2, hepatocellular carcinoma (HCC) type; MCF-7, Michigan Cancer Foundation-7; NT, compounds not tested; VEGFR, vascular endothelial growth factor receptor.

17.65 ± 0.16, and 20.58 ± 0.21 μM, respectively, whereas compounds **19**, **11** and **7**, with IC₅₀ = 22.39 ± 0.21, 23.84 ± 0.22, and 24.52 ± 0.24 μM, respectively, displayed good cytotoxicity.

Finally, the most potent six derivatives **6**, **9**, **8**, **10**, **15**, and **18** were tested for their cytotoxicity against normal Vero cell lines. The results revealed that the tested compounds have low toxicity against Vero normal cells with IC₅₀ values ranging from 15.45 to 23.59 μM. The cytotoxicity of these compounds against the cancer cell lines ranged from 4.25 to 16.57 μM. Compounds **6**, **8**, **9**, **10**, **15**, and **18** are, respectively, 1.13, 3.74, 4.18, 3.64, 2.81, and 2.00 times more toxic to HePG2 cancer cell lines than to Vero normal cells. Also, compounds **6**, **8**, **9**, **10**, **15**, and **18** are, respectively, 2.06, 1.58, 1.76, 2.54, 1.40, and 2.69 times more toxic to breast cancer cell lines (MCF-7) than to Vero normal cells.

2.5 | In vitro VEGFR-2 kinase assay

Furthermore, all the synthesized compounds, **5–19**, were evaluated for their inhibitory activities against VEGFR-2 by using an anti-phosphotyrosine antibody with the Alpha Screen system (PerkinElmer).^[31,33] The results were reported as a 50% inhibition concentration value (IC₅₀) calculated from the concentration-inhibition response curve and summarized in Table 2. Sorafenib was used as a positive control in this assay. The tested compounds displayed high-to-medium inhibitory activity with IC₅₀ values ranging from 0.12 ± 0.01 to 0.29 ± 0.02 μM. Among them, compound **10** was found to be the most potent derivative that inhibited VEGFR-2 at an IC₅₀ value of 0.12 ± 0.01 μM, which is nearly equipotent to sorafenib IC₅₀ value (0.10 ± 0.02 μM). Compounds **8** and **9** exhibited very good activity with the same IC₅₀ value of 0.13 ± 0.02 μM. Also, compounds **15** and **18** exhibited very good activity with IC₅₀ values of 0.14 ± 0.05 and 0.16 ± 0.02 μM. Also, compounds **6**, **5**, and **17** possessed very good VEGFR-2 inhibition with the same IC₅₀ value of 0.19 ± 0.02 μM, which is more than half the activity of sorafenib. Compounds **19** and **7** displayed good VEGFR-2 inhibition with IC₅₀ values of 0.25 ± 0.02 and 0.29 ± 0.02 μM, respectively. However, compound **13** displayed moderate VEGFR-2 inhibition with an IC₅₀ value of 0.33 ± 0.01 μM.

2.6 | Structure–activity relationship (SAR)

The preliminary SAR study has focused on the effect of inhibition of ATP-binding hydrophobic pocket by pyridine nucleus. The pyridine-derived compounds occupied the ATP hydrophobic pocket and formed H-bonds with the essential amino acid residue Cys919. However, different moieties with different lipophilicity and electronic nature were introduced to study their effects on anticancer activity. The presence of lipophilic 2-bromophenyl moieties attached to the pyridine ring increases the hydrophobic interactions with the active site. The data obtained revealed that the tested compounds displayed different levels of anticancer activities.

From the structure of the synthesized derivatives and the data shown in Table 2, we can divide these tested compounds into three groups. The first group is the pyridine-derived compounds *para*-substituted with phenyl group as in **5**, **6**, **11**, **13**, and **15**. The presence of NH₂ group attached to N-1 of pyridine ring condensed with 2-bromophenyl as in compound **15** exhibited higher activity than the free NH₂ as in **5** and **6** against HepG2, whereas in MCF-7, it showed lower activity than **5** and **6**, respectively. The presence of amino groups at position-1 and 3,5-dicyano groups as in compounds **5** and **6** displayed higher activity than only 3,5-dicyano groups like **11** and NH₂, 3-CN, and 5-ethyl ester as in **13** against HepG2, respectively. The 1,2-dihydropyridine **5** exhibited higher activity than 1,2,3,4-tetrahydropyridine **6** against HepG2 cell lines, whereas compound **6** showed higher activity than **5**, **15**, **13**, and **11** against MCF-7, respectively.

In the second group **7**, **8**, **9**, and **10**, the pyridine nucleus fused with triazole one. The triazolopyridine substituted with a phenyl group at position-2 as in compounds **10** and **9** exhibited higher activities than that substituted with methyl **8** and the unsubstituted one, **7**, against both HepG2 and MCF-7 cell lines, respectively. The 1,2,3,5-tetrahydro-triazolopyridine **10** showed higher activities than the 3,5-dihydro-triazolopyridine **9** against both HepG2 and MCF-7 cell lines, respectively.

In the third group **17**, **18**, and **19**, the pyridine nucleus was fused to the benzene ring to form quinoline derivative **17**. In compound **18**, the bioisostere pyran ring was fused to the benzene ring to form chromene derivative. Moreover, ring expansion of the pyridine ring occurred to form the bioisostere 1,2-diazepine derivative **19**. The chromene derivative **18** exhibited higher activities than the quinoline derivative **17** and 1,2-diazepine derivative **19** against both HepG2 and MCF-7 cell lines, respectively.

2.7 | In silico absorption, distribution, metabolism, excretion, and toxicity (ADMET) profile

In the present study, a computational study of the four most active compounds (**8**, **9**, **10**, and **15**) was conducted to determine the surface area and other physicochemical properties according to the directions of Lipinski's rule.^[53] Lipinski suggested that the absorption of a compound is more likely to be better if the molecule obeys at least three out of four of the following rules: (i) HB donor groups ≤ 5; (ii) HB acceptor groups ≤ 10; (iii) M. Wt < 500; (iv) logP < 5. In this study, whereas the reference anticancer agent doxorubicin violates three of Lipinski's rules, our derivatives **8**, **9**, **10**, and **15** obey all Lipinski's rules. All the highest active derivatives have a number of hydrogen-bonding acceptor groups 5 and/or 6 and only 1 and/or 2 hydrogen-bonding donors. Also, molecular weights are less than 500 and logP less than 5 and all these values agree with Lipinski's rules. Also, ADMET profiles of the newly synthesized derivatives were preliminarily assessed to analyze their potentials to build up as good medication candidates. Prediction of ADMET profiles was conducted with the aid of pkCSM descriptors algorithm protocol.^[54]

TABLE 3 ADMET profile of the four most active compounds and doxorubicin

Parameter	8	9	10	15	Doxorubicin
Molecular properties					
Molecular weight	345.167	418.254	416.238	450.296	543.525
LogP	2.50388	3.68896	3.86246	3.25126	0.0013
Rotatable bonds	1	2	2	4	5
Acceptors	5	6	5	5	12
Donors	1	2	1	1	6
Surface area	132.923	162.948	161.616	175.970	222.081
Absorption					
Water solubility	-3.261	-4.051	-3.276	-5.284	-2.915
CaCO ₂ permeability	0.572	0.45	0.477	0.717	0.457
Intestinal abs. (human)	83.944	93.321	91.333	88.569	62.372
Skin permeability	-2.77	-2.746	-2.735	-2.831	-2.735
P-glycoprotein substrate	Yes	Yes	Yes	No	Yes
P-glycoprotein I inhibitor	No	Yes	No	Yes	No
P-glycoprotein II inhibitor	No	Yes	Yes	Yes	No
Distribution					
VDss (human)	-0.346	-0.318	-0.617	-0.046	1.647
Fraction unbound (human)	0.143	0.018	0.05	0.0	0.215
BBB permeability	-1.117	0.089	-1.047	-0.793	-1.379
CNS permeability	-2.118	-1.67	-1.788	-2.144	-4.307
Metabolism					
CYP2D6 substrate	Yes	Yes	Yes	No	No
CYP3A4 substrate	Yes	Yes	Yes	Yes	No
CYP1A2 inhibitor	Yes	Yes	Yes	No	No
CYP2C19 inhibitor	No	Yes	Yes	Yes	No
CYP2C9 inhibitor	Yes	Yes	Yes	Yes	No
CYP2D6 inhibitor	No	No	No	No	No
CYP3A4 inhibitor	No	Yes	Yes	Yes	No
Excretion					
Total clearance	-0.049	-0.243	0.035	0.261	0.987
Renal OCT2 substrate	No	No	No	Yes	No
Toxicity					
AMES toxicity	No	Yes	Yes	No	No
Max. tolerated dose (human)	0.048	0.05	0.506	-0.243	0.081
hERG I inhibitor	No	No	No	No	No
hERG II inhibitor	Yes	Yes	Yes	No	Yes
Oral rat acute toxicity (LD ₅₀)	2.569	2.669	2.641	2.583	2.408
Oral rat chronic toxicity (LOAEL)	1.114	1.166	1.061	1.217	3.339
Hepatotoxicity	No	No	No	No	Yes

(Continues)

TABLE 3 (Continued)

Parameter	8	9	10	15	Doxorubicin
Skin sensitization	No	No	No	No	No
<i>Tetrahymena pyriformis</i> toxicity	0.403	0.446	0.286	1.409	0.285
Minnow toxicity	2.257	1.335	0.998	-0.633	4.412

Abbreviations: ADMET, absorption, distribution, metabolism, excretion, and toxicity; BBB, blood–brain barrier; CNS, central nervous system; VDss, volume of distribution at steady state.

After assessing ADMET profiles of compounds **8**, **9**, **10**, and **15** (Table 3), we can suggest that these derivatives have the advantage of better intestinal absorption in humans than doxorubicin (83.944–93.321), compared with 62.3 in the case of doxorubicin. This preference may be attributed to the superior lipophilicity of our designed ligands, which would make it easier to go along different biological membranes.^[55] Accordingly, they may have significant to good bioavailability after oral administration. Studying the central nervous system (CNS) permeability, our derivatives **8**, **9**, **10**, and **15** demonstrated the best ability to penetrate the CNS (CNS permeability values -1.67 to -2.144), whereas doxorubicin is unable to penetrate (CNS permeability < -4.0). It is also clear that the cytochrome P3A4, the main enzyme involved in drug metabolism, could be inhibited under the effect of compounds **9**, **10**, and **15**, whereas **8** and doxorubicin could not. This is also perhaps due to the higher lipophilicity of our new ligands **9**, **10**, and **15**. The total clearance is a significant parameter in deciding dose intervals as a tool for the assessment of excretion. Doxorubicin exhibited the highest total clearance value as compared with other ligands. However, new ligands showed lower total clearance values. Thus, doxorubicin could be excreted quicker and accordingly require shorter dosing intervals. Dissimilar to doxorubicin, new compounds exhibited slower clearance rates, which means the preference of possible extended dosing intervals of the novel derivatives. The last parameter examined in the ADMET profiles of our newly synthesized VEGFR-2 inhibitors is toxicity. As displayed in Table 3, all the new ligands showed no hepatotoxicity drawback, unlike doxorubicin that exhibited unwanted hepatotoxic effects. Finally, oral acute toxic doses of the new compounds (LD_{50}) are almost slightly more than the reference drug (2.569–2.669 for our new derivatives as compared with 2.408 of doxorubicin).

3 | CONCLUSION

In summary, 12 new pyridine-derived compounds **5–19** have been designed, synthesized, and evaluated for their anticancer activities against two human tumor cell lines, hepatocellular carcinoma (HepG2) and breast cancer (MCF-7), targeting the VEGFR-2 enzyme. All the tested compounds showed variable anticancer activities. The molecular design was performed to investigate the binding mode of the proposed compounds with

the VEGFR-2 receptor. Inhibition of the ATP-binding pocket of the VEGFR-2 receptor has an important effect on anticancer activities. Most of the prepared compounds displayed excellent-to-good growth inhibitory activity against the tested cancer cell lines. In particular, compounds **10**, **9**, **8**, and **15** were found to be the most potent derivatives over all the tested compounds against the HepG2 and MCF-7 cancer cell lines with $IC_{50} = 4.25 \pm 0.03$, $6.08 \pm 0.06 \mu\text{M}$, 4.68 ± 0.06 , $11.06 \pm 0.09 \mu\text{M}$, 4.34 ± 0.04 , $10.29 \pm 0.09 \mu\text{M}$ and 6.37 ± 0.06 , $12.83 \pm 0.13 \mu\text{M}$, respectively. Compound **10** exhibited higher activity against HepG2 than sorafenib ($IC_{50} = 9.18 \pm 0.6$ and $5.47 \pm 0.3 \mu\text{M}$, respectively) and doxorubicin ($IC_{50} = 7.94 \pm 0.6$ and $8.07 \pm 0.8 \mu\text{M}$, respectively). It also exhibited higher activity than doxorubicin against MCF-7 cancer cell lines but lower than sorafenib. Compounds **9**, **8**, and **15** exhibited higher activities than sorafenib and doxorubicin against HepG2 but exhibited lower activities against MCF-7 cancer cell lines. The most potent six derivatives **6**, **9**, **8**, **10**, **15**, and **18** were tested for their cytotoxicity against normal Vero cell lines. The results revealed that the tested compounds have low toxicity against Vero normal cells with IC_{50} values ranging from 15.45 to 23.59 μM . The cytotoxicity of these compounds against the cancer cell lines ranged from 4.25 to 16.57 μM . Compounds **6**, **8**, **9**, **10**, **15**, and **18** are, respectively, 1.13, 3.74, 4.18, 3.64, 2.81, and 2.00 times more toxic to HepG2 cancer cell lines than to Vero normal cells. Also, compounds **6**, **8**, **9**, **10**, **15**, and **18** are, respectively, 2.06, 1.58, 1.76, 2.54, 1.40, and 2.69 times more toxic to breast cancer cell lines (MCF-7) than to Vero normal cells. The tested compounds displayed high-to-medium inhibitory activity with IC_{50} values ranging from 0.12 ± 0.01 to $0.29 \pm 0.02 \mu\text{M}$. Among them, compound **10** was found to be the most potent derivative that inhibited VEGFR-2 at IC_{50} value of $0.12 \pm 0.01 \mu\text{M}$, which is nearly equipotent to sorafenib IC_{50} value of $0.10 \pm 0.02 \mu\text{M}$. Compounds **8** and **9** exhibited very good activity with the same IC_{50} value of $0.13 \pm 0.02 \mu\text{M}$. Also, compounds **15** and **18** exhibited very good activity with IC_{50} values of 0.14 ± 0.05 and $0.16 \pm 0.02 \mu\text{M}$. Also, compounds **6**, **5**, and **17** possessed very good VEGFR-2 inhibition with the same IC_{50} value of $0.19 \pm 0.02 \mu\text{M}$, which is more than half of the activity of sorafenib. Compounds **19** and **7** displayed good VEGFR-2 inhibition with IC_{50} values = 0.25 ± 0.02 and $0.29 \pm 0.02 \mu\text{M}$, respectively. However, compounds **13** displayed moderate VEGFR-2 inhibition with an IC_{50} value = $0.33 \pm 0.01 \mu\text{M}$.

4 | EXPERIMENTAL

4.1 | Chemistry

4.1.1 | General

Melting points of the reaction products were determined in open capillary tubes on an electrothermal melting point apparatus and were uncorrected. The Fourier Transform infrared measurements were recorded on a Perkin-Elmer Model 297 IR spectrometer using the KBr wafer technique at the Central Laboratory of Faculty of Science, Cairo University. The ^1H NMR (400 MHz) and ^{13}C NMR (100 MHz) spectra were recorded on a Varian Gemini spectrometer with chemical shift (δ) expressed in ppm downfield using tetramethylsilane as an internal standard at the main Defense Chemical Laboratory. Mass spectra were conducted using Shimadzu GC-MSQP 1000 EX instrument operating at 70 eV, and the elemental analyses were performed on a Perkin-Elmer 2400 CHN elemental analyzer at the Micro-analytical Center of Al-Azhar University. All reactions were monitored by thin-layer chromatography (TLC) and PTLC (1-mm layer thickness), which were conducted using pre-coated plates of silica gel 60 F254 (Merck), and spots were detected using a UV lamp (254 nm). The spots on TLC were visualized by warming with 5% cerium ammonium molybdate in 2 N H_2SO_4 -sprayed plates on a hot plate.

The InChI codes of the investigated compounds, together with some biological activity data, are provided as Supporting Information.

N'-(2-Bromobenzylidene)-2-cyanoacetohydrazide (4)

Equimolar amounts of 2-cyanoacetohydrazide **1** (0.99 g, 0.01 mol) and 2-bromobenzaldehyde **2** (1.85 ml, 0.01 mol) were synthesized according to Bondock et al.^[46] in 50 ml absolute ethanol, followed by addition of two to three drops of glacial acetic acid. The resulting mixture was magnetically stirred, while cold, for an hour. The reaction was examined by TLC. The precipitated product that formed was collected by filtration and crystallized from ethanol to give compound **4** with high purity. Compound **3** as white precipitate; yield (2.3 g, 95%); m.p. 150°C. IR (KBr, cm^{-1}): 3190 (NH), 3094 (CH arom.), 2960 (CH aliph.), 2264 ($\text{C}\equiv\text{N}$), 1675 ($\text{C}=\text{O}$), and 1587 ($\text{C}=\text{N}$); ^1H NMR (400 MHz, deuterated dimethyl sulfide [$\text{DMSO}-d_6$]) δ (ppm): 4.22 (s, 2H, CH_2), 7.32–7.97 (m, 4H, Ar-H), 8.49 (s, 1H, $\text{CH}=\text{N}$), and 11.95 (s, 1H, NH exchangeable with D_2O); ^{13}C NMR (100 MHz, $\text{DMSO}-d_6$) δ (ppm): 24.85, 116.45, 124.09, 127.79, 128.65, 130.57, 132.51, 133.62, 159.53, and 165.94. Anal. calcd. for $\text{C}_{10}\text{H}_8\text{BrN}_3\text{O}$ (266.10): C, 45.14; H, 3.03; N, 15.79%. Found: C, 45.10; H, 2.98; N, 15.75%.

1,6-Diamino-4-(2-bromophenyl)-2-oxo-1,2-dihydropyridine-3,5-dicarbonitrile (5)

Method A: A mixture of compound **4** (2.66 g, 0.01 mol) and malononitrile (0.66 ml, 0.01 mol) in absolute ethanol (20 ml) containing two drops of piperidine was refluxed for 5 h. The pale brown

precipitate obtained during heating was filtered and recrystallized from suitable solvents to give compound **5**.

Method B: A mixture of 2-(2-bromobenzylidene)malononitrile **2** (2.31 g, 0.01 mol) and 2-cyanoacetohydrazide **3** (0.99 g, 0.01 mol) in absolute ethanol (20 ml) containing two drops of piperidine was heated under reflux for 5 h. The pale brown precipitate obtained during heating was filtered and recrystallized from ethanol to give the targeted compound **5**. When the reaction mother liquor was heat-concentrated and left to cool, another solid product crop was obtained and known as product **6**.

Dehydrogenation of **6** leads to formation of **5**; the suspension of **6** (3.3 g, 0.01 mol) in trifluoroacetic acid was heated under reflux for 2 h. The solid product obtained was filtered, washed with diethyl ether, and crystallized from ethanol to give **5** as brown crystals; yield (2.31 g, 70%); m.p. 170°C. IR (KBr, cm^{-1}): 3407, 3313, 3210 (2 NH_2), 2957 (CH aliph.), 2207 (2 $\text{C}\equiv\text{N}$), and 1676 ($\text{C}=\text{O}$); ^1H NMR (400 MHz, $\text{DMSO}-d_6$) δ (ppm): 5.70 (s, 2H, N-NH₂ exchangeable with D_2O), 7.27–7.83 (m, 4H, Ar-H), and 8.60 (s, 2H, C-NH₂ exchangeable with D_2O); ^{13}C NMR (100 MHz, $\text{DMSO}-d_6$) δ (ppm): 75.40, 114.59, 116.01, 116.41, 120.81, 124.68, 128.73, 130.54, 132.14, 134.27, 136.31, 159.48, and 166.93; Anal. calcd. for $\text{C}_{13}\text{H}_8\text{BrN}_5\text{O}$ (330.15): C, 47.30; H, 2.44; N, 21.21%. Found: C, 47.44; H, 2.19; N, 21.38%.

1,6-Diamino-4-(2-bromophenyl)-2-oxo-1,2,3,4-tetrahydropyridine-3,5-dicarbonitrile (6)

Compound **6** as brown crystals; yield (1.66 g, 50%); m.p. 200°C. ^1H NMR (400 MHz, $\text{DMSO}-d_6$) δ (ppm): 3.02 (d, 1H, $\text{C}_4\text{-H}$), 3.06 (d, 1H, $\text{C}_3\text{-H}$), 4.56 (s, 2H, N-NH₂ exchangeable with D_2O), 7.01–7.62 (m, 4H, Ar-H), and 12.48 (s, 2H, C-NH₂ exchangeable with D_2O). Anal. calcd. for $\text{C}_{13}\text{H}_{10}\text{BrN}_5\text{O}$ (332.16): C, 47.01; H, 3.03; N, 21.08%. Found: C, 47.15; H, 2.79; N, 21.25%.

7-(2-Bromophenyl)-5-oxo-3,5-dihydro-[1,2,4]triazolo[1,5-a]pyridine-6,8-dicarbonitrile (7)

Stirring a mixture of ethyl chloroformate/*N,N*-dimethylformamide (30 ml, 1:5), compound **5** (3.3 g, 0.01 mol) was added gradually for half an hour, and then the reaction mixture was heated under reflux for 3 h. The reaction mixture was evaporated under reduced pressure and a solid product was triturated with methanol. The solidified product was filtered off and recrystallized from suitable solvents to give compound **7** as brown crystals; yield (2.24 g, 66%); m.p. 220°C. IR (KBr, cm^{-1}): 3322 (NH), 2951 (CH arom.), 2859 (CH aliph.), 2213 (2 $\text{C}\equiv\text{N}$), and 1675 ($\text{C}=\text{O}$); ^1H NMR (400 MHz, $\text{DMSO}-d_6$) δ (ppm): 7.09–7.92 (m, 4H, Ar-H), 8.26 (s, 1H, NH, exchangeable with D_2O), and 8.57 (s, 1H, $\text{CH}=\text{N}$); ^{13}C NMR (100 MHz, $\text{DMSO}-d_6$) δ (ppm): 115.07, 116.48, 117.96, 121.81, 128.72, 130.65, 131.52, 133.33, 136.30, 137.62, 153.30, 154.39, 159.45, and 162.77. Anal. calcd. for $\text{C}_{14}\text{H}_6\text{BrN}_5\text{O}$ (340.14): C, 49.44; H, 1.78; N, 20.59%. Found: C, 49.36; H, 1.73; N, 20.47%.

7-(2-Bromophenyl)-2-methyl-5-oxo-3,5-dihydro-[1,2,4]triazolo[1,5-a]pyridine-6,8-dicarbonitrile (8)

A mixture of **5** (3.3 g, 0.01 mol) and acetic anhydride (15 ml) was heated under reflux for 5 h. A solid product was filtered off and

recrystallized from suitable solvents to give compound **8** as pale brown crystals; yield (3.4 g, 97%), m.p. 240°C. IR (KBr, cm^{-1}): 3387 (NH), 3062 (CH arom.), 2970 (CH aliph.), 2126 (2 $\text{C}\equiv\text{N}$), and 1690 ($\text{C}=\text{O}$); ^1H NMR (400 MHz, $\text{DMSO-}d_6$) δ (ppm): 1.29 (s, 3H, CH_3), 7.05–7.89 (m, 4H, Ar-H), and 7.94 (s, 1H, NH, exchangeable with D_2O); ^{13}C NMR (100 MHz, $\text{DMSO-}d_6$) δ (ppm): 23.05, 114.52, 117.99, 120.38, 121.81, 127.89, 128.85, 130.49, 131.61, 133.67, 137.62, 157.86, 158.37, 158.77, and 168.32; Anal. calcd. for $\text{C}_{15}\text{H}_8\text{BrN}_5\text{O}$ (354.17); C, 50.87; H, 2.28; N, 19.77%. Found: C, 50.78; H, 2.15; N, 19.65%.

7-(2-Bromophenyl)-5-oxo-2-phenyl-1,2,3,5-tetrahydro-[1,2,4]-triazolo[1,5-a]pyridine-6,8-dicarbonitrile (9)

A mixture of **5** (3.3 g, 0.01 mol) and benzaldehyde (1.06 ml, 0.01 mol) in dioxane (50 ml) containing piperidine was heated under reflux for 3 h. A solid product was filtered off and recrystallized from suitable solvents to give compound **9** as pale brown crystals; yield (4 g, 95.7%), m.p. 130°C. IR (KBr, cm^{-1}): 3318, 3210 (2NH), 2957 (CH aliph.), 2314, 2207 (2 $\text{C}\equiv\text{N}$), and 1676 ($\text{C}=\text{O}$); ^1H NMR (400 MHz, $\text{DMSO-}d_6$) δ (ppm): 4.21 (s, 1H, $\text{C}_5\text{-H}$ triazol), 7.56–7.85 (m, 9H, Ar-H), 9.26 (s, 1H, C-NH, exchangeable with D_2O), 9.26, and 10.71 (s, 2H, N-NH+OH tautomeric exchangeable with D_2O); ^{13}C NMR (100 MHz, $\text{DMSO-}d_6$) δ (ppm): 10.95, 36.07, 38.82, 101.64, 123.71 (2), 128.07 (2), 128.44 (2), 130.08 (2), 132.91 (2), 137.61 (2), 143.50, 160.25, and 173.17 (2). Anal. calcd. for $\text{C}_{20}\text{H}_{12}\text{BrN}_5\text{O}$ (418.25); C, 57.43; H, 2.89; N, 16.74%. Found: C, 57.39%; H, 2.77%; N, 16.65%.

7-(2-Bromophenyl)-5-oxo-2-phenyl-3,5-dihydro-[1,2,4]triazolo[1,5-a]pyridine-6,8-dicarbo-nitrile (10)

A suspension of **9** (0.2 g) in trifluoroacetic acid (5 ml) was stirred at room temperature for 5 min and then poured into cold water. The solid product was filtered off and recrystallized from suitable solvents to give compound **10** as brown crystals; yield (4.16 g, 35.7%), m.p. 300°C. IR (KBr, cm^{-1}): 3182 (NH), 3090 (CH arom.), 2924 (CH aliph.), 2258, 2208 (2 $\text{C}\equiv\text{N}$), 1672 ($\text{C}=\text{O}$), and 1611 ($\text{C}=\text{N}$); ^1H NMR (400 MHz, $\text{DMSO-}d_6$) δ (ppm): 7.15–8.40 (m, 4H, Ar-H), and 8.46 (s, 1H, NH, exchangeable with D_2O); ^{13}C NMR (100 MHz, $\text{DMSO-}d_6$) δ (ppm): 116.26, 116.64, 118.63 (2), 123.26 (2), 123.87, 128.78 (2), 128.89, 129.02 (2), 131.71, 131.77, 131.87, 137.37, 137.41, 148.52, 162.38, and 166.36. Anal. calcd. for $\text{C}_{20}\text{H}_{10}\text{BrN}_5\text{O}$ (416.24); C, 57.71; H, 2.42; N, 16.83%. Found: C, 57.68; H, 2.38; N, 16.75%.

6-Amino-4-(2-bromophenyl)-2-oxo-1,2-dihydropyridine-3,5-dicarbonitrile (11)

To a suspension of **5** (3.3 g, 0.01 mol) in aqueous acetic acid (100 ml, 60%), sodium nitrite (0.015 mol in 5 ml water) was added. The reaction mixture was stirred at room temperature for 2 h and then left overnight. A solid product was filtered off and recrystallized from suitable solvents to give compound **11** as pale brown crystals; yield (1 g, 31.7%), m.p. 230°C. IR (KBr, cm^{-1}): 3406, 3300 (NH_2/NH), 2210 (2 $\text{C}\equiv\text{N}$), and 1691 ($\text{C}=\text{O}$); ^1H NMR (400 MHz, $\text{DMSO-}d_6$) δ (ppm): 5.67 (s, 2H, NH_2 , exchangeable with D_2O), 7.12–7.80 (m, 4H, Ar-H),

and 8.56 (s, 1H, NH, exchangeable with D_2O); ^{13}C NMR (100 MHz, $\text{DMSO-}d_6$) δ (ppm): 115.11 (2), 120.92, 123.90, 129.04, 129.26, 131.89, 137.39, 149.62, 149.74, 149.91, 157.47, and 168.49. Anal. calcd. for $\text{C}_{13}\text{H}_7\text{BrN}_4\text{O}$ (315.13); C, 49.55; H, 2.24; N, 17.78%. Found: C, 49.48; H, 2.15; N, 17.72%.

Ethyl 1,2-diamino-4-(2-bromophenyl)-5-cyano-6-oxo-1,6-dihydropyridine-3-carboxylate (13)

A mixture of **3** (2.66 g, 0.01 mol) and ethyl cyanoacetate (1.13 ml, 0.01 mol) in absolute ethanol (20 ml) containing two drops of triethylamine was heated under reflux for 5 h, and the reaction mixture was left to cool. The solid product obtained was filtered off and crystallized for purification from ethanol to give **13** as white powder; (1.9 g, 50.39%), m.p. 170°C. IR (KBr, cm^{-1}): 3399, 3290 (2 NH_2), 3078 (CH arom.), 2980 (CH aliph.), 2216 (CN), and 1651 ($\text{C}=\text{O}$); ^1H NMR (400 MHz, $\text{DMSO-}d_6$) δ (ppm): 1.19 (q, 2H, CH_2), 4.30 (t, 3H, CH_3), 5.70 (s, 2H, NH_2 exchangeable with D_2O), 7.20–7.65 (m, 4H, Ar-H), and 9.05 (s, 2H, NH_2 , exchangeable with D_2O); ^{13}C NMR (100 MHz, $\text{DMSO-}d_6$) δ (ppm): 14.24, 60.47, 90.96, 116.39, 120.75, 127.92, 128.92, 129.91, 130.26, 132.40, 133.24, 140.42, 158.48, 159.20, and 165.82. Anal. calcd. for $\text{C}_{15}\text{H}_{13}\text{BrN}_4\text{O}_3$ (377.20); C, 47.76%; H, 3.47%; N, 14.85%. Found: C, 47.85%; H, 3.63%; N, 14.66%.

6-Amino-1-[(2-bromobenzylidene)amino]-4-(4-methoxyphenyl)-2-oxo-1,2,3,4-tetrahydro-pyridine-3,5-dicarbonitrile (15)

A mixture of **3** (2.66 g, 0.01 mol), 2-(4-methoxybenzylidene) malononitrile (1.84 g, 0.01 mol), and 0.5 ml of triethylamine was refluxed in 30 ml of 1,4-dioxane for 5 h and then left to cool. The solid product formed was collected by filtration and recrystallized from ethanol to give compounds **15** as yellow powder; (2.25 g, 50%) m.p. 140°C. IR (KBr, cm^{-1}): 3347, 3202 (NH_2), 3078 (CH arom.), 2973 (CH aliph.), 2215 (2 CN), and 1699 ($\text{C}=\text{O}$); ^1H NMR (400 MHz, $\text{DMSO-}d_6$) δ (ppm): 3.22 (s, 3H, OCH_3), 3.81 (d, 1H, CH- Ar-H), 3.85 (d, 1H, CH-CN), 5.62 (s, 2H, NH_2 , exchangeable with D_2O), 6.97–7.54 (m, 8H, Ar-H), and 8.91 (s, 1H, $\text{CH}=\text{N}$); ^{13}C NMR (100 MHz, $\text{DMSO-}d_6$) δ (ppm): 25.61, 55.78, 114.17, 114.38, 114.38, 116.16, 117.04, 126.92, 127.83, 128.02, 128.49, 128.73, 129.04, 130.27, 130.61, 132.26, 132.53, 133.87, 157.09, 159.77, and 169.14. Anal. calcd. for $\text{C}_{21}\text{H}_{16}\text{BrN}_5\text{O}_2$ (450.30); C, 56.01%; H, 3.58%; N, 15.55%. Found: C, 56.15%; H, 3.55%; N, 15.65%.

2-[2-(2-Bromobenzylidene)hydrazinyl]-4-oxo-3,4-dihydroquinoline-3-carbonitrile (17)

A mixture of **3** (2.66 g, 0.01 mol) and anthranilic acid (1.38 g, 0.01 mol) in dioxane (30 ml) was refluxed for 2–6 h with a few drops of triethylamine. A solid product was obtained after cooling the reaction mixture to room temperature, which was filtered, dried, and recrystallized from suitable solvents to give compound **17**; (1.65 g, 45%) m.p. 170°C. IR (KBr, cm^{-1}): 3228 (NH), 3009 (CH arom.), 2996 (CH aliph.), 1701 ($\text{C}=\text{O}$), and 1587 ($\text{C}=\text{N}$); ^1H NMR (400 MHz, $\text{DMSO-}d_6$) δ (ppm): 1.38 (s, 1H, NH), 3.34 (s, 1H, CH), 7.44–7.99 (m, 8H, CH- aromatic ring), and 8.01 (s, 1H, $\text{CH}=\text{N}$); ^{13}C NMR

(100 MHz, DMSO-*d*₆) δ (ppm): 21.20, 38.43, 54.50, 116.08 (2), 129.47 (2), 129.81 (2), 131.27 (2), 131.83 (2), 133.89 (2), 155.60, and 162.27. Anal. calcd. for C₁₇H₁₁BrN₄O (367.21): C, 55.61; H, 3.02; N, 15.26%. Found: C, 55.58; H, 2.99; N, 15.14%.

N'-(2-Bromobenzylidene)-2-imino-2H-chromene-3-carbohydrazone (18)

A mixture of **3** (2.66 g, 0.01 mol) and salicylaldehyde (1.22 g, 0.01 mol) in dioxane (30 ml) was refluxed for 2–6 h with few drops of triethylamine. A solid product was obtained after cooling the reaction mixture to room temperature, which was filtered off, dried, and recrystallized from suitable solvents to give compound **18** as pale brown precipitate; yield (2 g, 54%) m.p. 120°C. IR (KBr, cm⁻¹): 3199 (NH), 3059 (CH arom.), 1693 (C=O), and 1614 (C=N); ¹H NMR (400 MHz, DMSO-*d*₆) δ (ppm): 6.93–8.15 (m, 8H, aromatic ring), 8.91 (s, 1H, CH=N), 8.94 (s, 1H, C=NH), 8.99 (s, 1H, CH pyrene), and 11.95 (s, H, NH, exchangeable with D₂O); ¹³C NMR (100 MHz, DMSO-*d*₆) δ (ppm): 113.96, 114.28, 114.69 (2), 128.46, 128.67 (2), 128.89, 130.31, 130.39, 130.61, 130.84, 135.21, 146.17, 155.64, 158.23, and 161.71. Anal. calcd. for C₁₇H₁₂BrN₃O₂ (370.21): C, 55.15; H, 3.27; N, 11.35%. Found: C, 55.08; H, 3.19; N, 11.29%.

5-Amino-7-(2-[2-bromobenzylidene]hydrazinyl)-3-oxo-2,3-dihydro-1H-1,2-diazepine-4-carbonitrile (19)

A mixture of **3** (2.66 g, 0.01 mol) and 2-cyanoacetohydrazide (0.99 g, 0.01 mol) in dioxane (30 ml) was heated under reflux for 2–6 h. A solid product was obtained after cooling, which in turn was filtered off and recrystallized from suitable solvents to give **19** as pale brown precipitate; yield (1 g, 30%) m.p. 200°C. IR (KBr, cm⁻¹): 3404, 3192 (NH₂/NH), 3055 (CH arom.), 2935 (CH aliph.), 2213 (CN), and 1654 (C=O); ¹H NMR (400 MHz, DMSO-*d*₆) δ (ppm): 4.89 (s, 1H, CH-diazepine), 6.86–7.93 (m, 6H, aromatic ring+NH₂), 8.42 (s, 1H, CH=N), 9.84 (s, 1H, C=NH), 10.17, and 12.00 (2s, 2H, NH+OH tautomeric); MS (*m/z*): 347.26 (1.17%), 346.11 (4.81%), 341.99 (18.84%), 339.93 (23.31%), and 261.09 (100%, base peak). Anal. calcd. for C₁₃H₁₁BrN₆O (347.18): C, 44.98%; H, 3.19%; N, 24.21%. Found: C, 44.87%; H, 3.23%; N, 24.36%.

ACKNOWLEDGMENTS

The authors extend their appreciation and thanks to Science Way for scientific research and consultations, Nasr city, Egypt. Also, the authors extend their appreciation and thanks to Dr. Fatma M. I. A. Shoman, MD in Clinical Pathology, Blood bank specialist, Blood bank directorate manager, Ministry of Health, Cairo, Egypt, for helping in the pharmacological part.

CONFLICTS OF INTEREST

The authors declare that there are no conflicts of interest.

ORCID

Adel A.-H. Abdel-Rahman  <http://orcid.org/0000-0003-3319-8191>

Mohamed M. Khalifa  <http://orcid.org/0000-0002-8146-993X>

Khaled El-Adl  <http://orcid.org/0000-0002-8922-9770>

REFERENCES

- [1] H. Chen, J. Kovar, S. Sissons, K. Cox, W. Matter, F. Chadwell, P. Luan, C. J. Vlahos, A. Schutz-Geschwender, D. M. Olive, *Anal. Biochem.* **2005**, 338, 136. <https://doi.org/10.1016/j.ab.2004.11.015>
- [2] P. Traxler, P. Furet, *Pharmacol. Ther.* **1999**, 82, 195. [https://doi.org/10.1016/s0163-7258\(98\)00044-8](https://doi.org/10.1016/s0163-7258(98)00044-8)
- [3] J. J. Cui, M. Tran-Dub, H. Shen, M. Nambu, P. P. Kung, M. Pairish, L. Jia, J. Meng, L. Funk, I. Botrous, M. McTigue, N. Grodsky, K. Ryan, E. Padrique, G. Alton, S. Timofeevski, S. Yamazaki, Q. Li, H. Zou, J. Christensen, B. Mroczkowski, S. Bender, R. S. Kania, M. P. Edwards, *J. Med. Chem.* **2011**, 54, 6342. <https://doi.org/10.1021/jm2007613>
- [4] M., Shibuya, L. Claesson-Welsh, *Exp. Cell Res.* **2006**, 312, 549. <https://doi.org/10.1016/j.yexcr.2005.11.012>
- [5] W. Gu, Y. Dai, H. Qiang, W. Shi, C. Liao, F. Zhao, W. Huang, H. Qian, *Bioorg. Chem.* **2017**, 72, 116. <https://doi.org/10.1016/j.bioorg.2017.04.001>
- [6] G. Guetz, B. Uzzan, P. Nicolas, M. Cucherat, J. Morere, R. Benamouzig, J. Breaux, G. Perret, *Br. J. Cancer* **2006**, 94, 1823.
- [7] A. Yuan, C. Yu, W. Chen, F. Lin, S. Kuo, K. Luh, P. Yang, *Int. J. Cancer* **2000**, 89, 475.
- [8] J. Jacobsen, K. Grankvist, T. Rasmuson, A. Bergh, G. Landberg, B. Ljungberg, *Br. J. Urol. Int.* **2004**, 93, 297.
- [9] N. Ferrara, *Oncology* **2005**, 69, 11.
- [10] S. Matsumoto, N. Miyamoto, T. Hirayama, H. Oki, K. Okada, M. Tawada, H. Iwata, K. Nakamura, S. Yamasaki, H. Miki, A. Hori, S. Imamura, *Bioorg. Med. Chem.* **2013**, 21(24), 7686. <https://doi.org/10.1016/j.bmc.2013.10.028>
- [11] T. Usui, H. S. Ban, J. Kawada, T. Hirokawa, H. Nakamura, *Bioorg. Med. Chem. Lett.* **2008**, 18, 285. <https://doi.org/10.1016/j.bmcl.2007.10.084>
- [12] K. H. Lee, B. R. Huang, *Eur. J. Med. Chem.* **2002**, 37, 333. [https://doi.org/10.1016/S0223-5234\(02\)01354-5](https://doi.org/10.1016/S0223-5234(02)01354-5)
- [13] M. A. Abdullaziz, H. T. Abdel-Mohsen, A. M. El Kerdawy, F. A. F. Ragab, M. M. Ali, S. M. Abu-Bakr, A. S. Girgis, H. I. E. I. Diwani, *Eur. J. Med. Chem.* **2017**, 136, 315. <https://doi.org/10.1016/j.ejmech.2017.04.068>
- [14] K. Okamoto, M. Ikemori-Kawada, A. Jestel, K. von Konig, Y. Funahashi, T. Matsushima, A. Tsuruoka, A. Inoue, J. Matsui, *ACS Med. Chem. Lett.* **2015**, 6, 89. <https://doi.org/10.1021/ml500394m>
- [15] A. M. Sayed, F. A. Taher, M. R. K. Abdel-Samad, M. S. A. El-Gaby, K. El-Adl, N. M. Saleh, *Bioorg. Chem.* **2021**, 108, 104669. <https://doi.org/10.1016/j.bioorg.2021.104669>
- [16] H. T. Abdel-Mohsen, M. A. Abdullaziz, A. M. E. Kerdawy, F. A. F. Ragab, K. J. Flanagan, A. E. E. Mahmoud, M. M. Ali, H. I. E. Diwani, M. O. Senge, *Molecules* **2020**, 25, 770. <https://doi.org/10.3390/molecules25040770>
- [17] P. Wu, T. E. Nielsen, M. H. Clausen, *Trends Pharmacol. Sci.* **2015**, 36, 422. <https://doi.org/10.1016/j.tips.2015.04.005>
- [18] S. Cai, H. Deng, Y. Chen, X. Wu, X. Guan, *Medicine* **2017**, 96, e8704. <https://doi.org/10.1097/MD.0000000000008704>
- [19] J. N. Ho, S. S. Byun, S. E. Lee, J. I. Youn, S. Lee, *Oncol. Rep.* **2019**, 41, 2482. <https://doi.org/10.3892/or.2019.7005>
- [20] J. Dietrich, C. Hulme, L. H. Hurley, *Bioorg. Med. Chem.* **2010**, 18, 5738. <https://doi.org/10.1016/j.bmc.2010.05.063>
- [21] S. Wilhelm, C. Carter, M. Lynch, T. Lowinger, J. Dumas, R. A. Smith, B. Schwartz, R. Simantov, S. Kelley, *Nat. Rev. Drug Discov.* **2006**, 5, 835. <https://doi.org/10.1038/nrd2130>
- [22] A. AbdelHaleem, A. O. Mansour, M. AbdelKader, R. K. Arafa, *Bioorg. Chem.* **2020**, 103, 104222. <https://doi.org/10.1016/j.bioorg.2020.104222>
- [23] A. S. Mostafa, K. B. Selim, *Eur. J. Med. Chem.* **2018**, 156, 304.
- [24] K. S. Kim, L. Zhang, R. Schmidt, Z. W. Cai, D. Wei, D. K. Williams, L. J. Lombardo, G. L. Trainor, D. Xie, Y. Zhang, Y. An, J. S. Sack, J. S. Tokarski, C. Darienzo, A. Kamath, P. Marathe, Y. Zhang,

- J. Lippy, R. Sr, Jeyaseelan, B. Wautlet, B. Henley, J. Gullo-Brown, V. Manne, J. T. Hunt, J. Fargnoli, R. M. Borzilleri, *J. Med. Chem.* **2008**, *51*, 5330. <https://doi.org/10.1021/jm800476q>
- [25] A. H. Abadi, D. A. Abouel-Ella, J. Lehmann, H. N. Tinsley, B. D. Gary, G. A. Piazza, M. Abdel-Fattah, *Eur. J. Med. Chem.* **2010**, *45*, 90. <https://doi.org/10.1016/j.ejmech.2009.09.029>
- [26] A. M. Serry, S. Luik, S. Laufer, A. H. Abadi, *J. Comb. Chem.* **2010**, *12*, 559. <https://doi.org/10.1021/cc1000488>
- [27] M. H. El-Shershaby, K. M. El-Gamal, A. H. Bayoumi, K. El-Adl, H. E. A. Ahmed, H. S. Abulkhair, *Arch. Pharm. (Weinheim, Ger.)* **2020**, *354*, e2000277. <https://doi.org/10.1002/ardp.202000277>
- [28] A. Turky, A. H. Bayoumi, F. F. Sherbiny, K. El-Adl, H. S. Abulkhair, *Mol. Divers.* **2020**, *10131*. <https://doi.org/10.1007/s11030-020-10131-0>
- [29] M. A. El-Zahabi, H. Sakr, K. El-Adl, M. Zayed, A. S. Abdelraheem, S. I. Eissa, H. Elkady, I. H. Eissa, *Bioorg. Chem.* **2020**, *104*, 104218. <https://doi.org/10.1016/j.bioorg.2020.104218>
- [30] K. El-Adl, A. A. El-Helby, H. Sakr, I. H. Eissa, S. S. A. El-Hddad, F. M. I. A. Shoman, *Bioorg. Chem.* **2020**, *102*, 104059. <https://doi.org/10.1016/j.bioorg.2020.104059>
- [31] I. H. Eissa, A. A. El-Helby, H. A. Mahdy, M. M. Khalifaa, H. A. Elnagar, A. B. M. Mehany, A. M. Metwaly, M. A. Elhendawy, M. M. Radwan, M. A. ElSohly, K. El-Adl, *Bioorg. Chem.* **2020**, *105*, 104380. <https://doi.org/10.1016/j.bioorg.2020.104380>
- [32] N. M. Saleh, M. S. A. El-Gaby, K. El-Adl, N. E. A. Abd El-Sattar, *Bioorg. Chem.* **2020**, *104*, 104350. <https://doi.org/10.1016/j.bioorg.2020.104350>
- [33] K. El-Adl, A. A. El-Helby, H. Sakr, R. R. Ayyad, H. A. Mahdy, M. Nasser, H. S. Abulkhair, S. S. A. El-Hddad, *Arch. Pharm. (Weinheim, Ger.)* **2021**, *354*, e202000279. <https://doi.org/10.1002/ardp.202000279>
- [34] K. El-Adl, H. Sakr, M. Nasser, M. Alswah, F. M. A. Shoman, *Arch. Pharm.* **2020**, *353*, e2000079. <https://doi.org/10.1002/ardp.202000079>
- [35] K. El-Adl, A. A. El-Helby, H. Sakr, S. S. A. El-Haddad, *Arch. Pharm.* **2020**, *353*, e2000068. <https://doi.org/10.1002/ardp.202000068>
- [36] A. A. El-Helby, H. Sakr, R. R. A. Ayyad, K. El-Adl, M. M. Ali, F. Khedr, *Anti-Cancer Agents Med. Chem.* **2018**, *18*, 1184. <https://doi.org/10.2174/1871520618666180412123833>
- [37] A. A. El-Helby, H. Sakr, I. H. Eissa, H. Abulkhair, A. A. Al-Karmalawy, K. El-Adl, *Arch. Pharm. (Weinheim, Ger.)* **2019**, *352*, 1900113. <https://doi.org/10.1002/ardp.201900113>
- [38] K. El-Adl, A. A. El-Helby, H. Sakr, A. Elwan, *Bioorg. Chem.* **2020**, *105*, 104399. <https://doi.org/10.1016/j.bioorg.2020.104399>
- [39] K. El-Adl, A. A. El-Helby, R. R. Ayyad, H. A. Mahdy, M. M. Khalifa, H. A. Elnagar, A. B. M. Mehany, A. M. Metwaly, M. A. Elhendawy, M. M. Radwan, M. A. ElSohly, I. H. Eissa, *Bioorg. Med. Chem.* **2020**, *29*, 115872. <https://doi.org/10.1016/j.bmc.2020.115872>
- [40] M. Li, X. Yu, W. Li, T. Liu, G. Deng, W. Liu, H. Liu, F. Gao, *Oncotarget* **2018**, *9*, 152. <https://doi.org/10.18632/oncotarget.22077>
- [41] H. Wang, B. Rao, J. Lou, J. Li, Z. Liu, A. Li, G. Cui, Z. Ren, Z. Yu, *Front. Cell. Dev. Biol.* **2020**, *8*, 8. <https://doi.org/10.3389/fcell.2020.00055>
- [42] L. Goyal, M. D. Muzumdar, A. X. Zhu, *Clin. Cancer Res.* **2013**, *19*, 2310. <https://doi.org/10.1158/1078-0432.CCR-12-2791>
- [43] Y. Zhang, X. Gao, Y. Zhu, D. Kadel, H. Sun, J. Chen, Q. Luo, H. Sun, L. Yang, J. Yang, Y. Sheng, Y. Zheng, K. Zhu, Q. Dong, L. Qin, *J. Exp. Clin. Cancer Res.* **2018**, *37*, 93. <https://doi.org/10.1186/s13046-018-0750-2>
- [44] R. Aesoy, B. C. Sanchez, J. H. Norum, R. Lewensohn, K. Viktorsson, B. Linderholm, *Mol. Cancer Res.* **2008**, *6*, 1630. <https://doi.org/10.1158/1541-7786.MCR-07-2172>
- [45] H. T. Fahmy, S. A. F. Rostom, A. A. Bekhit, *Arch. Pharm. (Weinheim, Ger.)* **2002**, *335*, 213. [https://doi.org/10.1002/1521-4184\(200205\)335:5%3C213::AID-ARDP213%3E3.0.CO;2-H](https://doi.org/10.1002/1521-4184(200205)335:5%3C213::AID-ARDP213%3E3.0.CO;2-H)
- [46] S. Bondock, A. El-Tarhoni, A. A. Fadda, *ARKIVOC* **2006**, *2006*, 113. <https://doi.org/10.3998/ark.5550190.0007.905>
- [47] M. Abdel-Megid, M. A. Ibrahim, Y. Gabr, N. M. El-Gohary, E. A. Mohamed, *J. Heterocyclic Chem.* **2013**, *50*, 615. <https://doi.org/10.1002/jhet.1608>
- [48] W. M. Basyouni, *Acta Chim. Slov.* **2003**, *50*, 223.
- [49] T. Nasr, S. Bondock, S. Eid, *Eur. J. Med. Chem.* **2014**, *84*, 491. <https://doi.org/10.1016/j.ejmech.2014.07.052>
- [50] G. A. Elsayed, S. A. Omara, R. M. Kamel, *J. Heterocyclic Chem.* **2017**, *54*, 3427. <https://doi.org/10.1002/jhet.2965>
- [51] F. M. Freimoser, C. A. Jakob, M. Aebi, U. Tuor, *Appl. Environ. Microbiol.* **1999**, *65*, 3727. <https://doi.org/10.1128/AEM.65.8.3727-3729.1999>
- [52] A. A. El-Helby, R. R. A. Ayyad, M. F. Zayed, H. S. Abulkhair, H. Elkady, K. El-Adl, *Arch. Pharm. (Weinheim, Ger.)* **2019**, *352*, e1800387. <https://doi.org/10.1002/ardp.201800387>
- [53] C. A. Lipinski, F. Lombardo, B. W. Dominy, P. J. Feeney, *Adv. Drug Deliv. Rev.* **1997**, *23*, 3. [https://doi.org/10.1016/S0169-409X\(96\)00423-1](https://doi.org/10.1016/S0169-409X(96)00423-1)
- [54] D. E. V. Pires, T. L. Blundell, D. B. Ascher, *J. Med. Chem.* **2015**, *58*, 4066. <https://doi.org/10.1021/acs.jmedchem.5b00104>
- [55] A. Beig, R. Agbaria, A. Dahan, *PLOS One* **2013**, *8*, e68237. <https://doi.org/10.1371/journal.pone.0068237>

SUPPORTING INFORMATION

Additional Supporting Information may be found online in the supporting information tab for this article.

How to cite this article: N. M. Saleh, A. A.-H. Abdel-Rahman, A. M. Omar, M. M. Khalifa, K. El-Adl. Pyridine-derived VEGFR-2 inhibitors: Rational design, synthesis, anticancer evaluations, in silico ADMET profile, and molecular docking. *Arch. Pharm.* **2021**;e2100085. <https://doi.org/10.1002/ardp.202100085>